Aalto University
School of Science
Master's Programme in Engineering Physics

Tuomas Toivo Kristian Pyhäranta

Thermodynamics and performance of cyclic quantum many-body heat engines

Master's Thesis
Espoo, March 6, 2020

Supervisor: Professor Christian Flindt
Advisor: Dr. Kay Brandner

Aalto University
School of Science
Master's Programme in Engineering Physics

ABSTRACT OF
MASTER'S THESIS

Author: Tuomas Toivo Kristian Pyhäranta

Title:
Thermodynamics and performance of cyclic quantum many-body heat engines

Date:	March 6, 2020	**Pages:**	57
Major:	Engineering Physics	**Code:**	SCI3056
Supervisor:	Professor Christian Flindt		
Advisor:	Dr. Kay Brandner		

In this thesis, we investigate the thermodynamics of quantum mechanical heat engines with non-interacting bosonic working fluids in harmonic potentials. Our main objectives are to investigate the performance effects of symmetric exchange interactions and non-adiabatic driving as well as to explore different methods for modelling the finite-time thermodynamics of periodically driven many-particle systems with Lindblad dynamics.

Starting from the study of ideal Otto cycles, whose unique features allow for the effects of Bose-Einstein condensation to be investigated with basic equilibrium thermostatistics, we predict a phase-transition induced power enhancement. Using this result as a benchmark, we develop a spectral technique for studying the linear-response thermodynamics of particle-conserving systems using a simple grand canonical framework, thus avoiding the technical difficulties typical to the canonical treatment of many-body systems. In the end, our results indicate that coherence cannot be harnessed to boost the power of Otto engines beyond quasi-classical performance. To complement the effectively canonical linear response theory, we also introduce a mean-field type formalism for studying population dynamics of many-body systems without having to solve the many-body Lindblad equation. This formalism can also be used to explore the thermodynamic behavior of quantum many-body heat engines.

Keywords: Quantum thermodynamics, Quantum heat engines, Bose-Einstein condensation, Many-body physics, Linear response, Mean-field theory

Language: English

Aalto-yliopisto
Perustieteiden korkeakoulu
Teknillisen fysiikan maisteriohjelma

DIPLOMITYÖN TIIVISTELMÄ

Tekijä:	Tuomas Toivo Kristian Pyhäranta		
Työn nimi:	Syklisten monikappalekvanttilämpövoimakoneiden termodynamiikka ja suorituskyky		
Päiväys:	6. maaliskuuta 2020	**Sivumäärä:**	57
Pääaine:	Teknillinen fysiikka	**Koodi:**	SCI3056
Valvoja:	Professori Christian Flindt		
Ohjaaja:	Tri Kay Brandner		

Tässä diplomityössä tarkastellaan kvanttimekaanisten lämpövoimakoneiden, joiden väliaine koostuu keskenään vuorovaikuttamattomista bosoneista, termodynamiikkaa. Työn päätavoitteina on tutkia symmetristen vaihtovuorovaikutusten ja epäadiabaattisen ajon vaikutusta lämpövoimakoneiden suorituskykyyn sekä erilaisia menetelmiä jaksollisesti ajettujen Lindblad-yhtälöä noudattavien avointen monikappalesysteemien termodynamiikan mallintamiseen.

Käyttämällä lähtökohtanamme Otto-työkiertoja, joiden ainutlaatuiset piirteet mahdollistavat Bosen-Einsteinin kondensaation vaikutuksen tutkimisen tavallisen termostatistiikan avulla, me ennustamme faasimuutoksen parantavan lämpövoimakoneen suorituskykyä. Tämä tulos toimii vertailukohtana kehittämällemme spektraalimenetelmälle, jonka avulla kanonisten systeemien termodynaamista vastetta voidaan tutkia suurkanonisessa yhteydessä. Menetelmän ansiosta tyypilliset monikappalesysteemien kanonisen käsittelyn kanssa vastaantulevat tekniset vaikeudet voidaan välttää. Tuloksemme osoittavat, että koherenssia ei voida hyödyntää Otto-lämpövoimakoneiden suorituskyvyn tehostamiseen klassisia rajoja pidemmälle. Kanonisen lineaarivasteteoriamme tueksi kehitämme myös keskeiskenttämenetelmän, joka mahdollistaa monikappalesysteemien tilapopulaatioiden aikakehityksen mallintamisen tiheysmatriisin Lindblad-yhtälöä ratkaisematta. Keskeiskenttäformalismiamme voidaan myös hyödyntää kvanttilämpövoimakoneiden termodynaamisen käyttäytymisen tutkimisessa.

Asiasanat:	kvanttitermodynamiikka, kvanttilämpövoimakoneet, Bosen-Einsteinin kondensaatio, monikappalefysiikka, lineaarinen vaste, keskeiskenttäteoria
Kieli:	englanti

Acknowledgements

I would like to express my sincere gratitude to Dr. Kay Brandner for his invaluable advice, counsel and support during the writing of this thesis and the work leading up to it. I also wish to thank Professor Christian Flindt for supervising this work and for providing me with the opportunity of carrying out the research included in this thesis as a member of his Quantum Transport group at Aalto University.

Espoo, March 6, 2020

Tuomas Toivo Kristian Pyhäranta

Contents

Chapter 1

Introduction

1.1 Background and motivation

In layman's terms, thermodynamics is the branch of physics exploring relationships between different forms of energy. The field emerged as a modern science during the Industrial Revolution out of a desire to improve the performance of mechanical heat engines, which are thermal machines converting heat into useful work and powering much of the industrialized world in doing so. Their operating principle was, and remains to this day, simple: by alternatingly coupling a working fluid with thermal reservoirs at different temperatures, heat is injected into the system, which is then compressed cyclically using a reciprocating piston with the induced pressure differences resulting in a net gain in mechanical power. Since the time of steam engines, thermodynamics has expanded into the study of chemical reactions [1], living organisms [2] and even information [3], yet heat engines nonetheless remain one of the main subjects of research within the field. These days, much of the theoretical interest in these devices is devoted to exploring thermodynamics in increasingly small systems, where thermal fluctuations play a critical role. Interestingly, the same laws of thermodynamics that imposed limits on the power and efficiency of steam engines in the 18^{th} century still govern the performance of today's nanoscopic heat engines based on colloidal particles [4–6].

However, as the miniaturization of heat engines has reached the atomic scale [7, 8] where systems are strongly influenced by quantum mechanical effects, there has been much recent discussion on the possibility of harnessing quantum phenomena to unlock non-classical means of energy conversion with hopes that the classical performance bounds might be overcome. As of now, bending classical laws of thermodynamics is mostly of theoretical interest with little practical value, but this is likely to change as scientific breakthroughs on the transport of heat in small systems are required for the realization of a commercial quantum computer. The connection between heat engines and quantum systems was first observed in a three-level maser [9], which was shown to

operate in its designated role as an amplifier only when its efficiency satisfied Carnot's theorem, the paradigmatic performance bound in thermodynamics. This connection has since then been extended to general open quantum systems [10], and today quantum heat engines form one of the primary branches of quantum thermodynamics, a relatively new field of physics attempting to generalize thermodynamic laws at the nanoscale by combining methods from classical stochastic thermodynamics and the theory of open quantum systems.

With the field of quantum thermodynamics still developing, the general performance effects of quantum phenomena remain poorly understood even for relatively well-studied effects in the context of heat engines. A prominent example is coherent superpositions between different states of the working fluid, which have been shown to have both beneficial [11–13] and detrimental [14–16] effects on performance depending on the physical details of the model. The research carried out on quantum heat engines has also mostly focused on ensembles of simple systems such as qubits and harmonic oscillators, and only recently have engines based on many-particle systems been considered. Nevertheless, important discoveries have already been made by exploring many-body engines. Notable highlights include a many-particle engine outperforming an ensemble of singe-particle engines with the same resources [17], utilizing the athermal properties of many-body-localized systems to perform thermodynamic tasks [18] as well as superradiance [19] and the conservation of collective quantities [20] leading to non-extensive scaling of the power output for many-particle engines. It was even conjectured in a recent paper that the Carnot efficiency could be reached with non-vanishing power, which would be a major deviation from the observed behavior of any known heat engine, by harnessing Bose-Einstein condensation [21].

The Bose-Einstein condensate, first predicted in 1925 [22] and experimentally observed in dilute gases in 1995 [23, 24], is a quantum mechanical state of matter that is formed when a bosonic fluid is cooled down to the point where the inter-particle spacing is of the order of the thermal wavelength of the particles. At this critical temperature, quantum effects become observable on a macroscopic scale as an anomalous population develops in the lowest energy state of the system following a second-order phase transition [25]. The mechanism for condensation is not even reliant on inter-bosonic interactions as the transition can be driven purely by the exchange symmetry of the particles, thus making condensation observable even in ideal gases. The consequent macroscopic manifestations of quantum effects, such as long-range order and wavefunction interference, are the main reason for the immense theoretical and experimental importance Bose-Einstein condensates have on modern condensed matter physics. The effect of Bose-Einstein condensation on the thermodynamic properties of quantum systems, however, is yet to be understood.

1.2 Objectives and scope

In this thesis, we have two primary objectives:

The first is to investigate the thermodynamic behavior of many-body heat engines in the quantum regime. We are particularly interested in the effect of symmetric exchange interactions and Bose-Einstein condensation on thermodynamic power; the qualitative impact of these two phenomena can be understood even under equilibrium conditions. To this end, it is instructive to consider relatively simple systems known to condense at low temperatures, and one of the simplest of such systems is the two-dimensional gas of non-interacting bosonic particles in a harmonic potential [26]. By operating the system as an Otto engine, whose operating cycle consists of two long isochoric strokes separated by instantaneous expansion and compression strokes [27], the unique structure of the Otto cycle can be used to express the thermodynamic figures of merit entirely in terms of differences in equilibrium energy. With the energy exchanges during the four individual strokes calculated, it becomes simple to establish how the periodic power scales with the system size in comparison with the performance of the quantum engine's classical counterpart. The characteristic features of the cycle also make it relatively simple to determine the effect of Bose-Einstein condensation on periodic power with nothing but basic thermostatistics: by choosing the temperatures of the heat sink and bath such that the system temperature crosses the critical value during the expansion and compression adiabats, leading to the fluid condensing and evaporating alternatingly during the thermodynamic cycle, the energy exchanges can be calculated without worrying about the non-analyticities in the free energy at the critical temperature.

We are also interested in the effects of quantum coherence on the thermodynamic performance of many-particle heat engines. As unperturbed pure states usually decohere into mixed states due to interactions with their environments [28], the effects of coherence can only be observed under finite-time driving, and there is no well-established standard technique for investigating the effects of non-adiabatic driving on quantum many-body heat engines. Hence, the second primary objective of this thesis is to explore methods for modelling the finite-time thermodynamics of open many-body systems under periodic driving. In a series of recent papers [29–34], master equations are used to model the non-equilibrium dynamics of quantum gases in various settings. Inspired in part by this approach, we investigate the finite-time many-body dynamics by introducing a thermodynamically consistent many-body master equation of the Lindblad form to describe the non-unitary time-evolution of many-body systems coupled to thermochemical reservoirs. This equation serves as a foundation for the subsequent studies of finite-time thermodynamics in this thesis. Like many-particle engines, many-body Lindblad equations have been another topic on which relatively little research has been conducted until quite recently [29, 30, 35], thus making this approach inherently interesting in itself.

As solving the master equation analytically is impossible under most circumstances, linear response provides us with an intuitive starting point for exploring finite-time thermodynamics perturbatively. A thermodynamically consistent linear response theory has been developed earlier for periodically driven canonical systems [36]. Many-body systems are, however, considerably easier to work with using the grand-canonical ensemble, which is considerably simpler in terms of mathematical complexity. The earlier linear response theory can be modified by first adding a chemical driving field and then introducing a spectral technique to constrain the chemical potential to impede the net particle exchange between the system and the reservoir. On a technical level, this can be achieved by expanding the full periodic state in the driving amplitudes and transitioning into Fourier space, where the Fourier modes of the particle current decouple as a result of the first-order expansion and where the resulting self-consistency condition can promptly be solved as a linear algebraic equation for the chemical potential, which becomes fully determined by the other driving fields. Due to the equivalence of ensembles in the thermodynamic limit [37], this allows for canonical many-particle systems to be described using the grand-canonical ensemble.

Although linear response makes it possible to explore the thermodynamic behavior of many-body engines analytically, the Lindblad equation can also be used to outline a fully numerical mean-field framework for the finite-time thermodynamics of driven-dissipative open quantum systems. The idea is to use mean-field methods to express the thermodynamic figures of merit in terms of ensemble averages and then apply the Lindblad equation to derive equations of motion for the mean-field variables. While the basic principle has been applied before using the canonical ensemble in [46], the canonical formulation of the method relies on several approximations and still leads to non-linear differential equations; in this thesis, we extend the idea to grand-canonical systems, where the more compact form of the Lindblad generator should produce linear equations. These mean-field equations of motion can then be solved numerically so long as a mechanism for enforcing the conservation of particles is implemented into the numerical routine to constantly vary the chemical potential along the cycle. Although our primary purpose is to complement the linear response theory, this method can be applied to any periodically driven system as no approximations beyond the usual ones made in the context of Lindblad dynamics are needed to derive the equations of motion. In principle, it should then be possible to explore the performance of coherent systems far from equilibrium without solving the Lindblad equation even approximately.

It is our goal to use these techniques to understand the thermodynamics and performance of cyclic quantum many-body heat engines. Although our research is limited to quantum mechanical Otto engines, which feature simple working cycles, the methods developed in this thesis are general and can be applied to a considerably wider scope of problems.

1.3 Content and structure

This thesis is structured as follows: Chapter 2 concerns quantum Otto engines operating in ideal cycles, where work and heat are fully determined by differences in equilibrium internal energy. As such, the chapter begins with a review of basic bosonic thermostatistics, which is then applied to study the thermodynamics of a many-body quantum Otto engine. The ideal Otto engine serves as a benchmark for the more involved cycles of later chapters. In the subsequent three chapters, we develop theory and methods for describing the time-evolution and quantum thermodynamics of periodically driven many-body systems. We introduce the many-body master equation and demonstrate its consistency with the established laws of thermodynamics in Chapter 3. Chapter 4 is used to treat the system thermodynamics perturbatively in the linear-response regime, while Chapter 5 is on the fully numerical mean-field-dynamics approach to finite-time thermodynamics. The thesis is concluded by Chapter 6, where the final results and conclusions are summarized. We also propose ways for improving our results and methods as well as possible directions for further research.

Chapter 2

Ideal many-body Otto engines

One of the main objectives of this thesis is to investigate how many-body phenomena affect the cyclic performance of quantum heat engines. For a basic qualitative understanding, it is sufficient to consider a relatively simple system: a quantum Otto heat engine based on a non-interacting boson gas. In ideal Otto cycles, comprising long isochoric strokes and instantaneous adiabats [27], all relevant figures of merit can be calculated under equilibrium conditions in terms of nothing but differences in internal energy, while basing the engine on a bosonic gas makes it possible to determine the thermodynamic differences between exchange-symmetric working fluids and their semi-classical counterparts, which are studied in Appendix A. Also, by confining the bosonic gas into a two-dimensional harmonic potential where condensation is known to occur [26], we can explore the effects of Bose-Einstein condensation on performance. The results of this chapter, obtained by studying ideal engines with equilibrium statistical mechanics, will serve as a benchmark for the more involved thermodynamic operating cycles of later chapters.

2.1 Thermostatistics of bosonic working fluids

We begin by reviewing basic bosonic thermostatistics in two-dimensional harmonic potentials. To avoid the considerable technical difficulties associated with the canonical partition function, which does not admit a simple analytic expression and can only be treated recursively [38], we work within a grand-canonical framework due to the simple and elegant expressions of the partition function and the thermodynamic potentials. This choice of statistical ensemble will be retained throughout this thesis.

The working fluid of the Otto engine consists of a finite number $\mathcal{N}$ of bosonic particles, trapped in a two-dimensional harmonic potential. The unitary single-particle dynamics

is generated by the Hamiltonian

$$h = \frac{\mathbf{p}^2}{2m} + \frac{1}{2}m\omega^2\mathbf{x}^2 \equiv \hbar\omega(\mathbf{a}^\dagger\mathbf{a} + 1), \tag{2.1}$$

where $\mathbf{p}$, $\mathbf{x}$ and $\mathbf{a} \equiv \sqrt{\frac{m\omega}{2\hbar}}(\mathbf{x} + \frac{\mathrm{i}}{m\omega}\mathbf{p})$ denote the two-dimensional momentum, position and annihilation operators [39]. By introducing the Fock-space operators $A^\dagger_{\mathbf{n}}$ and $A_{\mathbf{n}}$ that create and destroy particles in the single-particle eigenstate $|\mathbf{n}\rangle = |n_x, n_y\rangle$, the Hamiltonian for the full many-body system becomes [40]

$$H \equiv \sum_{\mathbf{m},\mathbf{n}} \langle\mathbf{m}|h|\mathbf{n}\rangle A^\dagger_{\mathbf{m}} A_{\mathbf{n}} = \sum_{\mathbf{n}} E_{\mathbf{n}} A^\dagger_{\mathbf{n}} A_{\mathbf{n}}, \tag{2.2}$$

where the single-particle eigenenergies are denoted by $E_{\mathbf{n}} \equiv \hbar\omega(n+1)$ with $n \equiv n_x + n_y$. This notation for the total number n of modes for the state $|\mathbf{n}\rangle = |n_x, n_y\rangle$ is used throughout this thesis. The eigenenergies of the two-dimensional potential are degenerate by the factor $g_n = n + 1$ [41]. Thus, apart from the symmetric exchange interactions between the bosons, the confined gas is non-interacting.

The thermostatistics of the gas is fully determined by the grand-canonical partition function $Z \equiv \mathrm{Tr}\{e^{-(H-\mu N)/T}\}$ [25], where Tr is the trace over the many-particle states and N the total particle number operator. The trace over the many-body Boltzmann factor yields

$$Z = \prod_{n=0}^{\infty} \left(1 - ze^{-\varepsilon_n/T}\right)^{-g_n}, \tag{2.3}$$

where T denotes temperature, $\varepsilon_n \equiv \hbar\omega n$ the energy difference separating the n^{th} energy level from the ground state and $z \equiv e^{\mu/T}$ the fugacity with the ground-state energy $\hbar\omega$ absorbed into the chemical potential μ. The partition sum in (2.3) normalizes the thermal distribution, defined by $R \equiv e^{-(H-\mu N)/T}/Z$ [28]. In this thesis, temperature is measured in units of energy as we have set Boltzmann's constant to one, leaving entropy dimensionless.

2.1.1 Chemical potential

To fix the mean number of particles to $\mathcal{N}$, the chemical potential must be such that $\sum_{\mathbf{n}}\langle A^\dagger_{\mathbf{n}} A_{\mathbf{n}}\rangle = \sum_n g_n \mathfrak{n}_n = \mathcal{N}$. Here, $\mathfrak{n}_n \equiv 1/(e^{(\hbar\omega n-\mu)/T} - 1) = 1/(e^{\hbar\omega n/T}/z - 1)$ is the Bose-Einstein factor, which gives the population for the eigenstates $|n_x, n_y\rangle$ with $n_x + n_y = n$ [25]. The sum over the Bose-Einstein factors does not admit an analytic expression. If, however, the gap between adjacent eigenenergies is small compared to the average energy of the gas particles, the sum over the number of modes can be replaced with an integral [25]. This approximation is valid if $\hbar\omega \ll T$, which is

certainly satisfied in the vapor phase. The ground-state contribution at $n = 0$ is not captured by the integral, so it must be included separately [25]:

$$\mathcal{N} = \mathfrak{n}_0 + \sum_{n=1}^{\infty} g_n \mathfrak{n}_n \simeq \frac{1}{1/z - 1} + \int_0^{\infty} \mathrm{d}n \, \frac{n+1}{e^{\hbar\omega n/T}/z - 1}. \tag{2.4}$$

The integral can be evaluated by expanding the Bose-Einstein factor into a power series and integrating term by term. Recalling the definition of the polylogarithm functions $\mathrm{Li}_s(z) \equiv \sum_{l=1} z^l/l^s$ [42], Equation (2.4) becomes

$$\mathcal{N} \simeq \mathrm{Li}_0(z) + \left(\frac{T}{\hbar\omega}\right) \mathrm{Li}_1(z) + \left(\frac{T}{\hbar\omega}\right)^2 \mathrm{Li}_2(z). \tag{2.5}$$

The chemical potential of confined, non-interacting bosons with finite mass must be negative so that the Bose-Einstein factors for all eigenstates sum up to a finite and positive number [25]. This value can be calculated numerically from Equation (2.5).

At high temperatures, where the particles occupy the excited states, the highest power of T in (2.5) dominates and the lower ones can be ignored. This term, however, involves no contribution from the ground state, which is given no weight in the integral by the term $n \cdot \mathfrak{n}_n$ of the integrand and which becomes macroscopically occupied at lower temperatures. In the thermodynamic limit, the energy cost of adding a particle into the system with a non-negligible ground-state population must approach the ground-state energy $\hbar\omega$, which corresponds to the effective chemical potential $\mu = 0$. Thus, the temperature below which the ground-state occupation begins to grow macroscopic can be approximated by the equation

$$\mathcal{N} = \left(\frac{T}{\hbar\omega}\right)^2 \mathrm{Li}_2(z = 1) = \left(\frac{T}{\hbar\omega}\right)^2 \zeta(2), \tag{2.6}$$

where the zeta function value $\zeta(2) = \pi^2/6$ [42]. Equation (2.6) yields an expression for the condensation temperature:

$$T_\mathrm{c} = \hbar\omega \frac{\sqrt{6\mathcal{N}}}{\pi}. \tag{2.7}$$

At this temperature, the system undergoes a phase transition known as Bose-Einstein condensation [25], where the ground state becomes macroscopically occupied. Below the critical temperature, the condensate fraction grows quadratically as temperature approaches zero in the thermodynamic limit [25].

The fugacity and ground-state population are plotted in Figure 2.1 against T/T_c for various mean particle numbers. From the scaling analysis in the figures, we find that the fugacity and the corresponding chemical potential develop non-analytic behavior at the critical temperature in the thermodynamic limit. As expected, the energy cost of adding a particle to the system approaches the ground-state energy as the ground-state population grows macroscopically large.

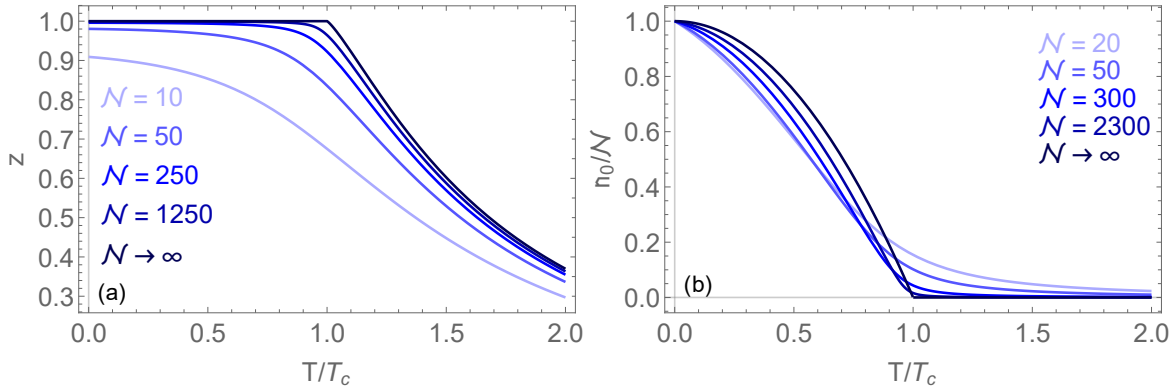

Figure 2.1: **(a)** The fugacity $z = e^{\mu/T}$ against T/T_c. In the thermodynamic limit, a kink develops at the condensation temperature $T/T_c = 1$ as the cost of adding a particle quasi-statically into the system approaches the ground-state energy and the system begins to condense. **(b)** The condensate fraction against T/T_c. Once temperature falls below the critical value, the fraction of particles in the ground state begins to grow quadratically as $T/T_c \to 0$ with $\mathfrak{n}_0/\mathcal{N} \simeq 1-(T/T_c)^2$ for $T/T_c < 1$ in the thermodynamic limit.

2.1.2 Internal energy

Similarly to the mean particle number, the internal energy $E \equiv \langle H \rangle = \mathrm{Tr}\{HR\}$ of the trapped bosonic gas

$$E = \sum_{\mathbf{n}} E_{\mathbf{n}} \langle A^\dagger_{\mathbf{n}} A_{\mathbf{n}} \rangle = \sum_{n=0}^{\infty} \frac{g_n \hbar\omega (n+1)}{e^{\hbar\omega n/T}/z - 1} \tag{2.8}$$

can be calculated explicitly using the integral approximation from Equation (2.4):

$$E/\hbar\omega \simeq \mathrm{Li}_0(z) + \left(\frac{T}{\hbar\omega}\right) \mathrm{Li}_1(z) + 2\left(\frac{T}{\hbar\omega}\right)^2 \mathrm{Li}_2(z) + 2\left(\frac{T}{\hbar\omega}\right)^3 \mathrm{Li}_3(z). \tag{2.9}$$

Here, the fugacity naturally satisfies the condition in Equation (2.5).

The internal energy per particle number is plotted as a function of the ratio T/T_c as well as the mean total particle number in Figure 2.2. As the thermodynamic limit is approached, the internal energy develops a kink at $T/T_c = 1$. Below the condensation temperature, the internal energy grows cubically in temperature, which can be explained with the behavior of the fugacity in Figure 2.1. The term with the highest power of $T/\hbar\omega$ in (2.9) dominates, so if the chemical potential is close to zero, the polylogarithm can be approximated by $\mathrm{Li}_3(z = 1) = \zeta(3)$ [42]. The internal energy is then given approximately by $E \simeq 2\zeta(3)(T/\hbar\omega)^3$. In the vicinity of the critical temperature, the dependence of E on T/T_c changes abruptly. At high temperatures, the energy curve settles into linear growth; this high-temperature behavior is consistent with the equipartition theorem [25].

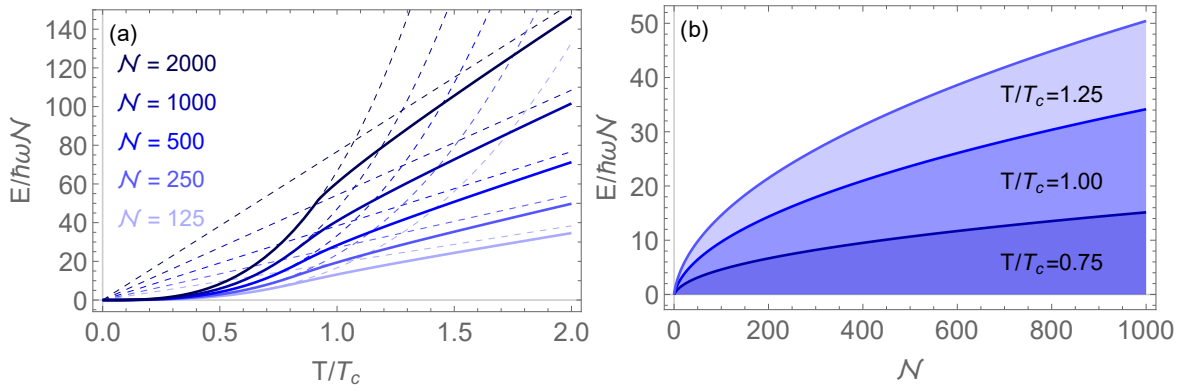

Figure 2.2: **(a)** Internal energy per bosonic particle against T/T_c. The limiting behavior is displayed in dashed lines with the cubic growth representing the condensate limit and the linear growth the semiclassical equipartition theorem. **(b)** Internal energy per bosonic particle against $\mathcal{N}$. The scaling is shown in three temperature regimes: below, at and above the condensation temperature. Note that only the ratio T/T_c has been fixed and not the base temperatures themselves; with T_c dependent on $\mathcal{N}$, both temperatures, base and critical, vary as the particle number is increased.

The observed scaling of the internal energy with $\sqrt{\mathcal{N}}$ can be explained with

$$\frac{T}{\hbar\omega} = \left(\frac{T}{T_c}\right)\frac{T_c}{\hbar\omega} = \left(\frac{T}{T_c}\right)\frac{\sqrt{6\mathcal{N}}}{\pi}. \tag{2.10}$$

As the internal energy is dominated by the highest order of $T/\hbar\omega$, the energy per particle must scale with $\mathcal{N}^{3/2}/\mathcal{N} = \sqrt{\mathcal{N}}$ when the ratio T/T_c is held constant.

2.2 Ideal Otto cycle

Having reviewed the thermostatistics of harmonically trapped Bose gases, we are now ready to apply it to study the cyclic thermodynamics of Otto engines. While classical Otto heat engines operate in cycles where the working fluid is alternatingly compressed and expanded with the fluid thermalizing with two bodies, one hot and the other cold, between these strokes [25], a quantum mechanical version of this engine can be realized through rapid modulation of the control parameters [27]. Specifically, by tuning the strength of the potential ω, an external controller can either extract or inject energy from or into the system as work, and the system is allowed to exchange heat with two heat baths at different temperatures between the instantaneous parameter quenches [27]. The role of the trap strength as a control parameter is thus analogous to the role of volume in classical Otto engines.

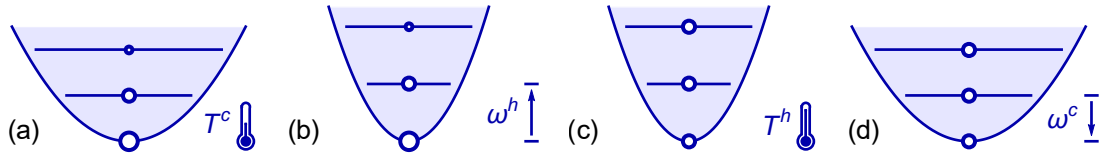

Figure 2.3: The four strokes of the Otto cycle [27]: In stroke 1, corresponding to the transition from **(a)** to **(b)**, the trap strength is instantaneously increased from $\omega^{\mathrm{c}} = \omega$ to $\omega^{\mathrm{h}} = \omega + \Delta\omega$ by the external controller, injecting energy W^{in} into the system. In stroke 2, corresponding to the transition from **(b)** to **(c)**, the system is brought into thermal contact with a heat source at the temperature $T^{\mathrm{h}} = T + \Delta T$ and allowed to equilibrate. Heat Q^{h} flows from the source to the system, which excites the particles that begin to occupy the higher energy levels. In stroke 3, **(c)** to **(d)**, the potential strength is reset to $\omega^{\mathrm{c}} = \omega$ and the working fluid performs work W^{out}. In stroke 4, **(d)** to **(a)**, the system transfers energy Q^{c} to a heat sink at $T^{\mathrm{c}} = T$ and thermalizes with it in the process while particles flow into the ground state. Note that the depicted populations in the diagrams are not to scale and are only used to illustrate the basic principle of the cycle.

2.2.1 The four strokes

The full operation cycle of the reciprocating quantum Otto engine, depicted schematically in Figure 2.3, consists of the following four strokes [27]:

① **Instantaneous compression.** The strength ω of the harmonic potential is instantaneously increased by $\Delta\omega$ with the external controller injecting work W^{in} into the system. As the stroke is carried out rapidly, the system remains in its initial state, described by the statistical operator ϱ_0, throughout the stroke.

② **Thermalization with heat source.** The system is brought into thermal contact with a heat source at the temperature $T + \Delta T$, resulting in the uptake of heat by the amount Q^{h}. After a time $\tau < \mathcal{T}$, where $\mathcal{T}$ is the period of the Otto cycle, of extracting heat from the source, the system is left in the state ϱ_τ.

③ **Instantaneous expansion.** The trap is reset instantaneously to its original strength ω with the engine performing work W^{out}. As in the compression stroke, the state of the bosonic working fluid remains unchanged at ϱ_τ due to the stroke being carried out instantaneously.

④ **Thermalization with heat sink.** The system is coupled to a heat sink at the temperature T for the time $\mathcal{T} - \tau$, dissipating heat Q^{c} and returning to the initial state ϱ_0.

2.2.2 Cyclic thermodynamics

As the Otto cycle is divided into four separate strokes, two isochoric and two adiabatic, the heat and work exchanges during the cycle are fully determined by differences in the internal energy E [27], which is a function of state [25]. If the cycle is ideal, i.e., sufficiently long for the system to equilibrate with the reservoirs in strokes 2 and 4, then $\varrho_0 = R|_{T,\omega} \equiv R_\mathrm{c}$ and $\varrho_\tau = R|_{T+\Delta T,\omega+\Delta\omega} \equiv R_\mathrm{h}$ are grand-canonical thermal states, which simplifies the expressions for the average energy considerably as they can now be evaluated in equilibrium.

Before we calculate the work and heat for the four strokes, we must note that the Hamiltonian is instantaneously changed from $H|_\omega \equiv H_\mathrm{c}$ to $H|_{\omega+\Delta\omega} \equiv H_\mathrm{h}$ and vice versa in strokes 1 and 3, respectively. Therefore, as the statistical operators remain unchanged during these instantaneous strokes, we need to calculate the mixed averages $\mathrm{Tr}\{H_\mathrm{c}R_\mathrm{h}\}$ and $\mathrm{Tr}\{H_\mathrm{h}R_\mathrm{c}\}$. This is done by deducing from Equation (2.1) that the single-particle Hamiltonians satisfy the identities

$$h_\mathrm{c} = \hbar(\omega+\Delta\omega)(\mathbf{a}_\mathrm{h}^\dagger\mathbf{a}_\mathrm{h}+1) - \hbar\frac{2\omega\Delta\omega+\Delta\omega^2}{4(\omega+\Delta\omega)}(\mathbf{a}_\mathrm{h}+\mathbf{a}_\mathrm{h}^\dagger)^2, \tag{2.11}$$

$$h_\mathrm{h} = \hbar\omega(\mathbf{a}_\mathrm{c}^\dagger\mathbf{a}_\mathrm{c}+1) + \hbar\frac{2\omega\Delta\omega+\Delta\omega^2}{4\omega}(\mathbf{a}_\mathrm{c}+\mathbf{a}_\mathrm{c}^\dagger)^2, \tag{2.12}$$

where $\mathbf{a}_\mathrm{c} \equiv (a_x, a_y)|_\omega$ and $\mathbf{a}_\mathrm{h} \equiv (a_x, a_y)|_{\omega+\Delta\omega}$ denote the vectorized annihilation operators for two-dimensional isotropic oscillators with frequencies ω and $\omega+\Delta\omega$, respectively. They are related through the definition

$$\mathbf{a}_\mathrm{h} \equiv \sqrt{\frac{\omega+\Delta\omega}{4\omega}}(\mathbf{a}_\mathrm{c}+\mathbf{a}_\mathrm{c}^\dagger) + \sqrt{\frac{\omega}{4(\omega+\Delta\omega)}}(\mathbf{a}_\mathrm{c}-\mathbf{a}_\mathrm{c}^\dagger). \tag{2.13}$$

Using the relations (2.11) and (2.12), the mixed averages can be calculated:

$$\mathrm{Tr}\{H_\mathrm{h}R_\mathrm{c}\} = \frac{1}{2}\left(1+(1+\Delta\omega/\omega)^{+2}\right)\mathrm{Tr}\{H_\mathrm{c}R_\mathrm{c}\} \simeq \left(1+\frac{\Delta\omega}{\omega}\right)\mathrm{Tr}\{H_\mathrm{c}R_\mathrm{c}\}, \tag{2.14}$$

$$\mathrm{Tr}\{H_\mathrm{c}R_\mathrm{h}\} = \frac{1}{2}\left(1+(1+\Delta\omega/\omega)^{-2}\right)\mathrm{Tr}\{H_\mathrm{h}R_\mathrm{h}\} \simeq \left(1-\frac{\Delta\omega}{\omega}\right)\mathrm{Tr}\{H_\mathrm{h}R_\mathrm{h}\}. \tag{2.15}$$

Here, the binomial approximations $(1+\Delta\omega/\omega)^{\pm 2} \simeq 1 \pm 2\Delta\omega/\omega$ hold when $\Delta\omega/\omega \ll 1$ [42]. Also, the sums can again be approximated by replacing them with integrals [25]. Using the heat engine sign convention, i.e., assigning a positive sign to work done by the system, the work and heat exchanges become

$$\begin{aligned} W^\mathrm{in} &= \mathrm{Tr}\{H_\mathrm{c}R_\mathrm{c}\} - \mathrm{Tr}\{H_\mathrm{h}R_\mathrm{c}\} < 0, \quad Q^\mathrm{h} = \mathrm{Tr}\{H_\mathrm{h}R_\mathrm{h}\} - \mathrm{Tr}\{H_\mathrm{h}R_\mathrm{c}\} > 0, \\ W^\mathrm{out} &= \mathrm{Tr}\{H_\mathrm{h}R_\mathrm{h}\} - \mathrm{Tr}\{H_\mathrm{c}R_\mathrm{h}\} > 0, \quad Q^\mathrm{c} = \mathrm{Tr}\{H_\mathrm{c}R_\mathrm{c}\} - \mathrm{Tr}\{H_\mathrm{c}R_\mathrm{h}\} < 0. \end{aligned} \tag{2.16}$$

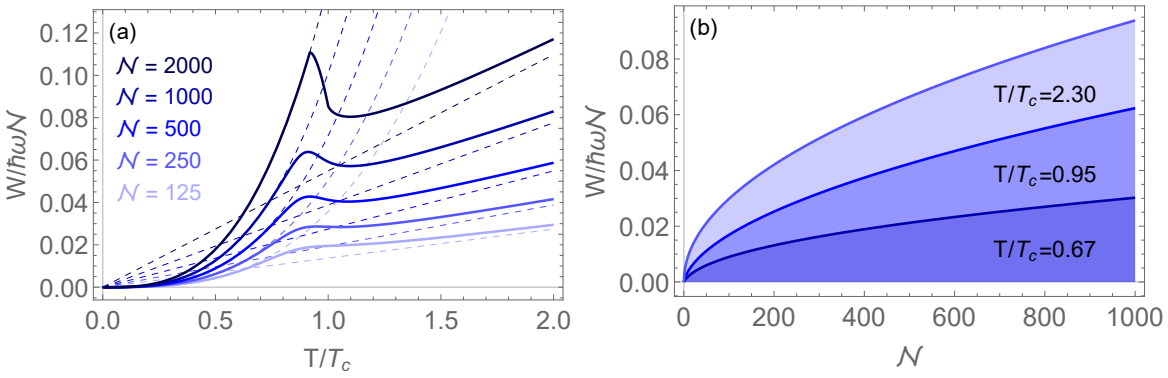

Figure 2.4: **(a)** The average cyclic work per particle against $T/T_{\rm c}$. A performance enhancement develops when the working fluid undergoes a phase transition during the cycle. Again, the dashed lines display the high-temperature and low-temperature limits. **(b)** The average cyclic work per particle against $\mathcal{N}$. The three temperatures correspond to both isochores taking place in the condensate phase ($T/T_{\rm c} = 0.67$), one taking place in the condensate and the other in the vapor phase ($T/T_{\rm c} = 0.95$), and the full cycle taking place in the vapor phase ($T/T_{\rm c} = 2.30$). Note that we have fixed $\Delta T/T = 1/10$ and $\Delta\omega/\omega = 1/100$. Also, only the ratios $T/T_{\rm c}$ are held constant in **(b)** and not the temperatures themselves.

Using the mixed-average expressions, the cyclic work can be written in terms of the equilibrium averages of energy as

$$\begin{aligned} W =& \frac{1-(1+\Delta\omega/\omega)^{+2}}{2}\mathrm{Tr}\{H_{\rm c}R_{\rm c}\} + \frac{1-(1+\Delta\omega/\omega)^{-2}}{2}\mathrm{Tr}\{H_{\rm h}R_{\rm h}\} \\ \simeq& \frac{\Delta\omega}{\omega}\left(\mathrm{Tr}\{H_{\rm h}R_{\rm h}\} - \mathrm{Tr}\{H_{\rm c}R_{\rm c}\}\right). \end{aligned} \tag{2.17}$$

Consistency with the second law of thermodynamics requires that trap and reservoir parameters must be chosen such that the efficiency $\eta \equiv W/Q^{\rm h}$ is bounded from above by the Carnot efficiency $\eta_{\rm C}$ [25]. If the difference between the trap strengths is small, the efficiency of the cycle is given approximately by

$$\eta = 1 - \frac{\mathrm{Tr}\{H_{\rm c}(R_{\rm h}-R_{\rm c})\}}{\mathrm{Tr}\{H_{\rm h}(R_{\rm h}-R_{\rm c})\}} \simeq 1 - \frac{\omega}{\omega+\Delta\omega} \leq 1 - \frac{T}{T+\Delta T} \equiv \eta_{\rm C}, \tag{2.18}$$

Since the Otto-cycle efficiency is fully determined by the trap strengths, efficiency will not be considered further in this thesis.

The net periodic work per bosonic particle is shown in Figure 2.4 against $T/T_{\rm c}$ and $\mathcal{N}$. We notice a condensation-induced deviation from expected behavior between $T^\star \equiv T_{\rm c}/(1+\Delta T/T)$, where the temperature gradient $\Delta T/T$ has been fixed, and the critical point. The observed temperature-dependence is explained by that the cyclic work is fully determined by changes in internal energy: when both reservoirs have temperatures

either above or below the condensation temperature, the work depends on temperature just like the internal energy, i.e., either linearly or cubically, and when the working fluid is in the vapor phase during the expansion stroke and in the condensate phase during the compression stroke, the work involves contributions roughly proportional to both T and T^3. This also explains the scaling of work with $\sqrt{\mathcal{N}}$.

Physically, this temperature-dependence implies that as the temperature of the cold reservoir is lowered slightly below the critical value, the cyclic net work experiences a phase-transition induced enhancement. In the phase-transition regime between $T^\star$ and T_c, the system condenses during the cold isochore and then evaporates during the hot one. As such, the engine starts the cycle with a significant condensate fraction. When the trap is stiffened during stroke 1, the internal energy change is comparatively small, since a large share of the bosons still occupies the ground state with little energy. Therefore, the work injected into the system $W^{\mathrm{in}} < 0$ is also small. During stroke 2, energy from the heat source excites the particles in the ground state, thus raising the internal energy and leaving the ground-state occupation level negligible. As a result, the engine performs a considerable amount of work $W^{\mathrm{out}} > 0$ during the instantaneous expansion in stroke 3 as the energy of the excited bosons collapses along with the internal energy. The working fluid is then coupled with the heat sink in stroke 4 and starts to condense. It should also be noted that the power also exceeds the semiclassical limit at the higher temperatures in the region $T < T^*$, where the ground-state population changes rapidly with temperature. As in the phase-transition regime, this also results in extreme differences in the ground-state occupation between strokes 1 and 3. At very low temperatures, where the particles in the condensate constitute a majority, the mean energy is always low enough for the semiclassical performance limit to be beyond reach.

The results of Figure 2.4 can be summarized as follows: while there is no difference in the scaling of power with system size between quantum systems and their semiclassical equivalents, we have established that it is possible to harness Bose-Einstein condensation to boost the engine power beyond the limits on performance imposed by semiclassical statistics. Physically, this is explained by the extreme differences in the ground-state occupations during the expansion and compression strokes, respectively, which are a direct consequence of the condensation. These results, derived with basic equilibrium statistical mechanics, form a consistency check for our studies of finite-time thermodynamics in the limit of long cycles.

Chapter 3

Many-body master equation

In general, the time-evolution of a closed quantum system in a pure state, represented by a wavefunction in the Hilbert space of the system, is determined by the Schrödinger equation [39]. The Schrödinger equation preserves the purity of the state as well as the mean energy in a constant potential, but once an isolated system is coupled with its surrounding environment, the system begins to decohere into a statistical mixture of pure states, also known as a mixed state, and the system can no longer be represented by a vector in the Hilbert space [28]. Instead, to account for the non-unitary influence of the environment, a statistical operator must be introduced to describe the system [28]. As quantum heat engines are open systems subject to external driving fields, which cause the mean energy to vary in time, introducing a master equation for the statistical operator to describe the many-body dynamics becomes crucial for the modelling of finite-time heat engines.

Accordingly, our primary objective in this chapter is to formulate the many-particle master equation. By focusing on the weak-coupling regime, the equation can be written in Lindblad form, which is the most general structure preserving the Hermiticity, positivity and trace of the statistical operator [43, 44]. As this many-body Lindblad equation forms the basis for exploring the finite-time thermodynamics of Otto cycles, our secondary objective is demonstrating the thermodynamic consistency of the master equation. Continuing with the grand-canonical approach, which allows for the results of the previous chapter to be used as a benchmark, we prove the stationarity of the equilibrium distribution. Also, to conclude the chapter, the canonical flux-force formulation of irreversible thermodynamics [45] is deployed for a perturbative description of entropy production, which the second law requires to be positive [25].

3.1 Lindblad dynamics

Our objective is to formulate a master equation to describe the many-body dynamics of confined, non-interacting boson gases with Hamiltonians of the form

$$H_t = \sum_{\mathbf{n}} E_{\mathbf{n},t} A^\dagger_{\mathbf{n},t} A_{\mathbf{n},t}, \tag{3.1}$$

where the sum runs over the single-particle energy eigenstates with corresponding eigenvalues $E_{\mathbf{n},t}$. The Fock-space operators $A_{\mathbf{n},t}$ and $A^\dagger_{\mathbf{n},t}$ remove and add particles from and to the eigenstate $|\mathbf{n}_t\rangle$, respectively [40]. The many-body Hamiltonian $H_{t+\mathcal{T}} = H_t$ is made explicitly time-dependent by external driving fields, which are operated with $\mathcal{T}$-periodic protocols.

We assume the system to be weakly coupled to a thermochemical reservoir with periodically operated temperature T_t and chemical potential μ_t. The time-evolution of the system, represented by the statistical operator ϱ_t, is generated by a Lindblad superoperator, i.e., $\dot{\varrho}_t = \hat{\mathsf{L}}_t \varrho_t \equiv \hat{\mathsf{H}}_t \varrho_t + \hat{\mathsf{D}}_t \varrho_t$, where $\hat{\mathsf{H}}_t \varrho_t \equiv -\mathrm{i}[H_t, \varrho_t]/\hbar$ denotes the standard Liouvillian and where the dissipation superoperator has the structure [28]

$$\hat{\mathsf{D}}_t \bullet \equiv \sum_{\mathbf{n}} \gamma_{\mathbf{n},t} \left(A_{\mathbf{n},t} \bullet A^\dagger_{\mathbf{n},t} - \frac{1}{2}\{\bullet, A^\dagger_{\mathbf{n},t} A_{\mathbf{n},t}\} \right) + \gamma^\dagger_{\mathbf{n},t} \left(A^\dagger_{\mathbf{n},t} \bullet A_{\mathbf{n},t} - \frac{1}{2}\{\bullet, A_{\mathbf{n},t} A^\dagger_{\mathbf{n},t}\} \right). \tag{3.2}$$

At this point, it should be emphasized that we have chosen to use the Fock operators $A_{\mathbf{n},t}$ and $A^\dagger_{\mathbf{n},t}$ as the Lindblad operators in such a way that the total mean particle number $\sum_{\mathbf{n}} \langle A^\dagger_{\mathbf{n},t} A_{\mathbf{n},t} \rangle$ is not conserved. Although it is possible to find such Lindblad operators, e.g., by second-quantizing the oscillator operators a_α and $a^\dagger_\alpha$, that the mean particle number remains constant, the resulting long operator strings would render both linear response and the mean-field-dynamics approach to finite-time thermodynamics intractable [46]; these two methods will be discussed in further detail in Chapters 4 and 5. Working with the grand-canonical ensemble, on the other hand, allows the comparison of subsequent results with Chapter 2 for consistency checks also well below the thermodynamic limit, where the ensembles are not equivalent [37]. Hence, the transitions between different eigenstates are treated indirectly in Equation (3.2) by assuming they happen through the particle reservoir.

The Lindblad form of the master equation is sufficient to ensure that the statistical operator ϱ_t will remain positive, Hermitian and trace-normalized as it evolves in time [43, 44]. Also, due to micro-reversibility, the quantum detailed-balance condition

$$\hat{\mathsf{D}}_t R_t = R_t \hat{\mathsf{D}}^\dagger_t, \tag{3.3}$$

where $\hat{\mathsf{D}}_t^\dagger$ denotes the adjoint dissipator

$$\hat{\mathsf{D}}_t^\dagger \bullet \equiv \sum_{\mathbf{n}} \gamma_{\mathbf{n},t} \left(A_{\mathbf{n}}^\dagger \bullet A_{\mathbf{n},t} - \frac{1}{2}\{\bullet, A_{\mathbf{n},t}^\dagger A_{\mathbf{n},t}\} \right) + \gamma_{\mathbf{n},t}^\dagger \left(A_{\mathbf{n},t} \bullet A_{\mathbf{n},t}^\dagger - \frac{1}{2}\{\bullet, A_{\mathbf{n},t} A_{\mathbf{n},t}^\dagger\} \right), \tag{3.4}$$

is implied in the absence of magnetic fields for the instantaneous grand-canonical equilibrium state $R_t \equiv e^{-K_t/T_t}/Z_t$ [36] with $K_t \equiv H_t - \mu_t N_t$ denoting the effective Hamiltonian operator for the many-body system.

3.2 Thermodynamics

Having introduced the many-body Lindblad equation, we now need to demonstrate that the derived dynamics are thermodynamically consistent. The second law requires that the total rate of entropy production must remain non-negative at all times, a condition that is met if the equilibrium operator R_t is a stationary solution of the Lindblad equation [47].

3.2.1 Stationary solution

To prove that the grand-canonical state R_t is a stationary solution, we use the bosonic commutation relation $[A_{\mathbf{n},t}, A_{\mathbf{m},t}^\dagger] = \delta_{\mathbf{mn}}$ [40] and the general identity $e^{\sum_\alpha X_\alpha} = \prod_\alpha e^{X_\alpha}$ for commuting operators $\{X_\alpha\}$ to expand the Boltzmann factor into a product of exponentials, which leads to

$$A_{\mathbf{n},t} R_t = R_t e^{+\xi_{\mathbf{n},t} A_{\mathbf{n},t}^\dagger A_{\mathbf{n},t}/T_t} A_{\mathbf{n},t} e^{-\xi_{\mathbf{n},t} A_{\mathbf{n},t}^\dagger A_{\mathbf{n},t}/T_t}, \tag{3.5}$$

where we have introduced the shorthand notation $\xi_{\mathbf{n},t} \equiv E_{\mathbf{n},t} - \mu_t$. This expression can be further simplified with the Baker-Hausdorff lemma [39], according to which $e^{sX} Y e^{-sX} = e^{s\hat{\mathsf{X}}} Y$ with $\hat{\mathsf{X}} \bullet \equiv [X, \bullet]$, for the commutation identities

$$A_{\mathbf{n},t} R_t = R_t A_{\mathbf{n},t} e^{-\xi_{\mathbf{n},t}/T_t}, \qquad A_{\mathbf{n},t}^\dagger R_t = R_t A_{\mathbf{n},t}^\dagger e^{+\xi_{\mathbf{n},t}/T_t}. \tag{3.6}$$

These relations can be used to re-write the action of the dissipation superoperator on the thermal state as

$$\hat{\mathsf{D}}_t R_t = \sum_{\mathbf{n}} A_{\mathbf{n},t} R_t A_{\mathbf{n},t}^\dagger (\gamma_{\mathbf{n},t} - \gamma_{\mathbf{n},t}^\dagger e^{\xi_{\mathbf{n},t}/T_t}) + A_{\mathbf{n},t}^\dagger R_t A_{\mathbf{n},t} (\gamma_{\mathbf{n},t}^\dagger - \gamma_{\mathbf{n},t} e^{-\xi_{\mathbf{n},t}/T_t}), \tag{3.7}$$

which vanishes identically if the rates satisfy the detailed-balance condition

$$\gamma_{\mathbf{n},t}^\dagger = \gamma_{\mathbf{n},t} e^{-\xi_{\mathbf{n},t}/T_t}. \tag{3.8}$$

Since the Fock-space operators $\{A_{\mathbf{n},t}, A_{\mathbf{n},t}^\dagger\}$ form an irreducible and self-adjoint set, the thermal state can be expected to be the unique stationary solution of the many-body master equation [47].

3.2.2 Entropy production

The second law also requires that the total entropy increases [25]. To develop the thermodynamics of the system, we begin with the first law

$$\dot{E}_t = J_t^E - P_t, \tag{3.9}$$

where E_t is the internal energy of the system, J_t^E the energy uptake from the reservoir and P_t the extracted power. Using that $E_t = \mathrm{Tr}\{H_t \varrho_t\}$ with $\varrho_{t+\mathcal{T}} = \varrho_t$ being the periodic state of the many-body system, we find

$$J_t^E = \mathrm{Tr}\{H_t \dot{\varrho}_t\} = \mathrm{Tr}\{(\hat{\mathsf{D}}_t^\dagger H_t)\varrho_t\} \qquad \text{and} \qquad P_t = \mathrm{Tr}\{\dot{H}_t \varrho_t\}. \tag{3.10}$$

Particle conservation requires that $\partial_t \langle N \rangle = J_t^\rho$, where $\langle N \rangle \equiv \mathrm{Tr}\{N R_t\}$ is the mean particle number in the system and

$$J_t^\rho \equiv \mathrm{Tr}\{N \dot{\varrho}_t\} = \mathrm{Tr}\{(\hat{\mathsf{D}}_t^\dagger N)\varrho_t\} \tag{3.11}$$

the particle uptake from the reservoir. It should be noted that the total particle number operator N can always be written in a time-independent basis; it is, therefore, a constant of motion.

We now formulate the second law. The rate of entropy production in the reservoir is given by

$$\sigma_t^{\mathrm{env}} = -(J_t^E - \mu_t J_t^\rho)/T_t, \tag{3.12}$$

while the rate of entropy production in the system reads

$$\sigma_t^{\mathrm{sys}} = -\mathrm{Tr}\{\dot{\varrho}_t \log \varrho_t\} = -\mathrm{Tr}\{(\hat{\mathsf{D}}_t \varrho_t) \log \varrho_t\}. \tag{3.13}$$

With $K_t = H_t - \mu_t N$, the total rate of entropy production can be re-written as

$$\sigma_t^{\mathrm{tot}} = -\mathrm{Tr}\{(\hat{\mathsf{D}}_t \varrho_t)\,(K_t/T_t + \log \varrho_t)\} = \mathrm{Tr}\{(\hat{\mathsf{D}}_t \varrho_t)(\log R_t - \log \varrho_t)\} \geq 0. \tag{3.14}$$

The inequality follows from Spohn's theorem [47], according to which the non-negativity of entropy production is respected by the Lindblad dynamics, since $\hat{\mathsf{D}}_t R_t = 0$ as a consequence of the detailed-balance relation. Hence, we have $\sigma_t^{\mathrm{tot}} = \sigma_t^{\mathrm{env}} + \sigma_t^{\mathrm{sys}} \geq 0$ for the total rate of entropy production.

3.2.3 Perturbation theory

To develop a perturbation theory consistent with the laws of thermodynamics, it is instructive to first introduce the canonical flux-force formulation of irreversible thermodynamics [45]. To this end, we parameterize the temperature and the chemical potential of the reservoir according to

$$T_t \equiv \frac{T(T + \Delta T)}{T + \Delta T(1 - f_t^q)} \qquad \text{and} \qquad \mu_t \equiv \mu + \Delta\mu\, f_t^\rho. \tag{3.15}$$

Here, f_t^q and f_t^ρ denote dimensionless driving fields assuming values between 0 and 1. Furthermore, T, μ, ΔT and $\Delta\mu$ are the base values of the reservoir temperature and chemical potential and their variation amplitudes, respectively. The entropy production in the reservoir is thus determined by the rate

$$\begin{aligned}\sigma_t^{\mathrm{env}} =& \left(\frac{\Delta T}{T(T+\Delta T)} f_t^q - \frac{1}{T}\right)\left(J_t^E - (\mu + \Delta\mu\, f_t^\rho)\, J_t^\rho\right) \\ \equiv& F^q\left(f_t^q J_t^E - f_t^q\,(\mu + \Delta\mu\, f_t^\rho)\, J_t^\rho\right) - \frac{1}{T} J_t^E + \frac{\mu}{T} J_t^\rho + F^\rho f_t^\rho J_t^\rho\end{aligned} \tag{3.16}$$

with the thermodynamic forces

$$F^q \equiv \frac{\Delta T}{T(T+\Delta T)} = \frac{1}{T} - \frac{1}{T+\Delta T}, \qquad F^\rho \equiv \Delta\mu/T. \tag{3.17}$$

We now separate the Hamiltonian $H_t = H + \Delta H\, G_t^w$ into a time-independent part H and a dimensionless periodic perturbation G_t^w with amplitude ΔH. Using that $\oint \mathrm{d}t\, J_t^\rho = 0$ and

$$\oint \mathrm{d}t\, J_t^E = -\Delta H \oint \mathrm{d}t\, \mathrm{Tr}\{\dot{G}_t^w \varrho_t\} \equiv -\Delta H\, J^w, \tag{3.18}$$

averaging σ_t^{env} yields

$$\sigma^{\mathrm{env}} \equiv \oint \mathrm{d}t\, \sigma_t^{\mathrm{env}} = F^q J^q + F^w J^w + F^\rho J^\rho. \tag{3.19}$$

Here, $\oint \mathrm{d}t \equiv \frac{1}{\mathcal{T}} \int_0^{\mathcal{T}} \mathrm{d}t$ denotes the period average, while the third thermodynamic force is defined as

$$F^w \equiv \Delta H/T. \tag{3.20}$$

Also, we have introduced the generalized thermodynamic fluxes

$$J^q \equiv \oint \mathrm{d}t \left[J_t^E - (\mu + \Delta\mu\, f_t^\rho)\, J_t^\rho\right] f_t^q, \;\; J^w \equiv \oint \mathrm{d}t\, \mathrm{Tr}\{\dot{G}_t^w \varrho_t\}, \;\; J^\rho \equiv \oint \mathrm{d}t\, f_t^\rho J_t^\rho. \tag{3.21}$$

As the von Neumann entropy is a function of state [25], we have $\oint \mathrm{d}t\, \sigma_t^{\mathrm{sys}} = 0$, and the canonical bilinear form of the total entropy production per cycle [45] becomes

$$\sigma \equiv \oint \mathrm{d}t\, \sigma_t^{\mathrm{tot}} = F^q J^q + F^w J^w + F^\rho J^\rho. \tag{3.22}$$

Chapter 4

Linear response theory

The many-body master equation introduced in the previous chapter forms the basis for exploring finite-time Otto engines. However, the thermodynamic fluxes depend crucially on the statistical operator satisfying the Lindblad equation, which is usually impossible to solve exactly. Therefore, perturbative methods are needed to investigate the finite-time thermodynamics of many-particle systems without resorting to numerical methods. Continuing with the canonical flux-force formulation, this chapter focuses on weakly driven systems, and linear response is a natural starting point for the study of such systems as extensive research has been devoted to the thermodynamics of periodically driven open quantum systems earlier [15, 36].

Since the number of particles is not conserved by the many-particle master equation from Chapter 3, our main objectives are finding a chemical potential protocol to impede the net particle exchange between the system and the reservoir on the average level as well as testing the validity of the resulting effectively canonical linear response theory by applying it to Otto engines. In the long-time limit, the linear response theory should produce results consistent with the results of Chapter 2, while the effects of coherence should become apparent under fast driving.

4.1 Linear-response ansatz

We begin by making the linear-response ansatz and assume that the system settles into the periodic state

$$\varrho_t = \exp\left[-K/T + \sum_{\alpha=q,w,\rho} F^\alpha Y_t^\alpha\right]/Z_t. \tag{4.1}$$

Here, Y_t^α denote the corrections due to thermal (q), mechanical (w) and chemical (ρ) driving fields. To expand the generalized fluxes to first order in the thermodynamic

forces, we apply the derivative formula for the exponential map [48]

$$\frac{\mathrm{d}}{\mathrm{d}t}e^{Y_t} = \int_0^1 \mathrm{d}s\, e^{sY_t}\dot{Y}_t e^{(1-s)Y_t} \tag{4.2}$$

to the linear-response ansatz for the periodic state of the system ϱ_t to get

$$\begin{aligned}\varrho_t &= R + \int_0^1 \mathrm{d}s\, R^s \sum_\alpha F^\alpha Y_t^\alpha R^{1-s} + \mathcal{O}(F^2) \\ &= R + \int_0^1 \mathrm{d}s\, R^s \sum_\alpha F^\alpha \delta Y_t^\alpha R^{1-s} + \mathcal{O}(F^2),\end{aligned} \tag{4.3}$$

where $\delta Y_t^\alpha \equiv Y_t^\alpha - \langle Y_t^\alpha \rangle$ denote deviations from the thermal ensemble averages.

Similarly, we can expand the full Lindblad generator

$$\hat{\mathsf{L}}_t = \hat{\mathsf{L}} + \sum_\alpha \hat{\mathsf{L}}_t^\alpha F^\alpha + \mathcal{O}(F^2) \tag{4.4}$$

in the thermodynamic forces and then substitute the result into the time derivative $\dot{\varrho}_t = \hat{\mathsf{L}}_t \varrho_t$ of Equation (4.3) to obtain the general result

$$\int_0^1 \mathrm{d}s\, R^s \sum_\alpha \delta\dot{Y}_t^\alpha F^\alpha R^{1-s} = \int_0^1 \mathrm{d}s\, R^s \sum_\alpha \hat{\mathsf{L}}^\ddagger \delta Y_t^\alpha F^\alpha R^{1-s} + \sum_\alpha \hat{\mathsf{L}}_t^\alpha R F^\alpha + \mathcal{O}(F^2), \tag{4.5}$$

where we have defined the superoperator $\hat{\mathsf{L}}^\ddagger \equiv \hat{\mathsf{H}} + \hat{\mathsf{D}}^\dagger$ and where the quantum detailed-balance condition was used to move the free generator, which satisfies $\hat{\mathsf{L}}R = 0$, in front of the perturbative correction δY_t^α.

The inhomogeneous part of Equation (4.5) still poses an obstacle for solving the periodic state. To simplify the equations, we note that the instantaneous equilibrium state is a stationary solution of the full Lindblad equation, i.e., $\hat{\mathsf{L}}_t R_t = 0$. If the driving amplitudes are small,

$$K_t/T_t = K/T - KF^q f_t^q + F^w G_t^w - NF^\rho f_t^\rho + \mathcal{O}(F^2) \tag{4.6}$$

and

$$\varrho_t = R + \int_0^1 \mathrm{d}s\, R^s \left(F^q f_t^q \delta K - F^w \delta G_t^w + F^\rho f_t^\rho \mu\, \delta N\right) R^{1-s} + \mathcal{O}(F^2). \tag{4.7}$$

Hence, we can identify

$$\hat{\mathsf{L}}_t^q R = -f_t^q \hat{\mathsf{L}}^\ddagger \delta K \equiv \hat{\mathsf{L}}^\ddagger \delta G_t^q, \qquad \hat{\mathsf{L}}_t^w R = \hat{\mathsf{L}}^\ddagger \delta G_t^w, \qquad \hat{\mathsf{L}}_t^\rho R = -f_t^\rho \hat{\mathsf{L}}^\ddagger \delta N \equiv \hat{\mathsf{L}}^\ddagger G_t^\rho. \tag{4.8}$$

Here, we introduced the new variables $G_t^q \equiv -f_t^q K$ and $G_t^\rho \equiv -f_t^\rho N$. Inserting these results into the differential equations for the perturbations δY_t^α and separating independent contributions from one another leads to

$$\delta\dot{Y}_t^q = \hat{\mathsf{L}}^\ddagger \delta Y_t^q - f_t^q \hat{\mathsf{L}}^\ddagger \delta K, \quad \delta\dot{Y}_t^w = \hat{\mathsf{L}}^\ddagger \delta Y_t^w + \hat{\mathsf{L}}^\ddagger \delta G_t^w, \quad \delta\dot{Y}_t^\rho = \hat{\mathsf{L}}^\ddagger \delta Y_t^\rho - f_t^\rho \hat{\mathsf{L}}^\ddagger \delta N, \quad (4.9)$$

which we can solve subject to periodic boundary conditions in analytic terms:

$$\delta Y_t^\alpha = \int_0^\infty \mathrm{d}\tau \, e^{\hat{\mathsf{L}}^\ddagger \tau} \hat{\mathsf{L}}^\ddagger \delta G_{t-\tau}^\alpha. \quad (4.10)$$

The resulting full periodic state is

$$\varrho_t = R + \sum_\alpha F^\alpha \int_0^1 \mathrm{d}s \, R^s \left(\int_0^\infty \mathrm{d}\tau \, e^{\hat{\mathsf{L}}^\ddagger \tau} \hat{\mathsf{L}}^\ddagger \delta G_{t-\tau}^\alpha \right) R^{1-s} + \mathcal{O}(F^2). \quad (4.11)$$

Note that the improper integral is well-defined if the stationary state R_t is unique, as we assume throughout, since δG_t^α are orthogonal to R_t by construction.

4.2 Kinetic coefficients

The result in (4.11) enables us to evaluate the thermodynamic fluxes in the linear-response regime. To this end, we introduce the Kubo correlation functions [49]

$$\langle\!\langle X, Y \rangle\!\rangle \equiv \int_0^1 \mathrm{d}s \, \langle \delta X R^s \delta Y R^{-s} \rangle = \int_0^1 \mathrm{d}s \, \left(\langle X R^s Y R^{-s} \rangle - \langle X \rangle \langle Y \rangle \right). \quad (4.12)$$

We will also use that $\hat{\mathsf{D}}^\dagger \hat{\mathsf{H}} = \hat{\mathsf{H}} \hat{\mathsf{D}}^\dagger$ as implied by the quantum detailed-balance condition. Plugging the periodic state (4.11) into the definitions of the thermodynamic fluxes (3.21) and using the periodicity of the system as well as basic properties of trace, the fluxes can be integrated by parts for the Onsager relations [36]

$$J^\alpha = \sum_\beta L^{\alpha\beta} F^\beta, \qquad \text{where} \qquad L^{\alpha\beta} \equiv \oint \mathrm{d}t \int_0^\infty \mathrm{d}\tau \, \langle\!\langle \dot{G}_t^\alpha, e^{\hat{\mathsf{L}}^\ddagger \tau} \hat{\mathsf{L}}^\ddagger G_t^\beta \rangle\!\rangle. \quad (4.13)$$

As seen from Equation (4.8), the thermal and chemical perturbation operators factorize according to $G_t^\alpha \equiv f_t^\alpha g^\alpha$ with

$$g^q \equiv -K \qquad \text{and} \qquad g^\rho \equiv -N. \quad (4.14)$$

If the mechanical perturbation also factorizes, i.e., if $G_t^w \equiv f_t^w g^w$ with f_t^w being a periodic and dimensionless driving field, the generalized kinetic coefficients can be expressed in the compact form

$$L^{\alpha\beta} = \oint \mathrm{d}t \int_0^\infty \mathrm{d}\tau \, \dot{f}_t^\alpha f_{t-\tau}^\beta \dot{\chi}_\tau^{\alpha\beta}, \quad (4.15)$$

where we have defined the linear-response functions, which depend only on the bare perturbations g^α, as

$$\chi_t^{\alpha\beta} \equiv \langle\!\langle g^\alpha, e^{\hat{\mathsf{L}}^\ddagger t} g^\beta \rangle\!\rangle. \tag{4.16}$$

With the Kronecker delta identity $\delta_{kl} = \oint \mathrm{d}t\, e^{\mathrm{i}(k-l)\Omega t}$ and the definition $\Omega \equiv 2\pi/\mathcal{T}$, simple Fourier decompositions $f_t^\alpha = \sum_{k=-\infty}^{\infty} c_k^\alpha e^{\mathrm{i}k\Omega t}$ of the driving fields can be used to express the kinetic coefficients as sums in Fourier space:

$$L^{\alpha\beta} = \mathrm{i}\Omega \sum_{k=-\infty}^{\infty} k c_k^\alpha \tilde{\chi}_{-k}^{\alpha\beta} c_{-k}^\beta. \tag{4.17}$$

Here, we have defined the integral transformation

$$\tilde{\chi}_k^{\alpha\beta} \equiv \int_0^\infty \mathrm{d}\tau\, \dot{\chi}_\tau^{\alpha\beta} e^{-\mathrm{i}k\Omega\tau}. \tag{4.18}$$

4.3 Effectively canonical systems

So far, our analysis has only been used to describe systems that exchange particles with chemical reservoirs. On an effective level, however, it can easily be extended to periodically driven systems with conserved particle numbers by choosing the time-dependent chemical potential such that there is no net particle exchange between the system and the thermochemical reservoir at any point in the cycle. To implement this self-consistency condition, we require that the instantaneous particle flux J_t^ρ vanishes identically at all times, regardless of the mechanical and thermal driving fields.

The first step in doing so is to re-write the particle flux J_t^ρ into an explicitly field-dependent form. As the quantum Liouvillian $\hat{\mathsf{H}}$ has no contribution to the trace due to the commutator, $J_t^\rho = -\mathrm{Tr}\{(\hat{\mathsf{D}}^\dagger \delta g^\rho)\varrho_t\} = -\mathrm{Tr}\{(\hat{\mathsf{L}}^\ddagger \delta g^\rho)\varrho_t\}$. Plugging in the full periodic state and integrating by parts leads to

$$J_t^\rho = \sum_\alpha \int_0^1 \mathrm{d}s\, \mathrm{Tr}\left\{\delta g^\rho R^s \left(\hat{\mathsf{L}}^\ddagger \delta G_t^\alpha - \int_0^\infty \mathrm{d}\tau\, \hat{\mathsf{L}}^\ddagger e^{\hat{\mathsf{L}}^\ddagger \tau} \delta \dot{G}_{t-\tau}^\alpha\right) R^{1-s}\right\} F^\alpha, \tag{4.19}$$

an expression which can be simplified with the factorization $G_t^\alpha = f_t^\alpha g^\alpha$ for

$$J_t^\rho = \sum_\alpha \int_0^1 \mathrm{d}s\, \left(\langle \delta g^\rho R^s \hat{\mathsf{L}}^\ddagger \delta g^\alpha R^{-s}\rangle f_t^\alpha - \int_0^\infty \mathrm{d}\tau\, \dot{f}_{t-\tau}^\alpha \dot{\chi}_\tau^{\rho\alpha}\right) F^\alpha. \tag{4.20}$$

We can now identify $\dot{\chi}_0^{\alpha\beta} = \int_0^1 \mathrm{d}s\, \langle \delta g^\alpha R^s \hat{\mathsf{L}}^\ddagger \delta g^\beta R^{-s}\rangle$. Hence, the self-consistency condition $J_t^\rho \stackrel{!}{=} 0$ reads

$$F^\rho \left(\dot{\chi}_0^{\rho\rho} f_t^\rho - \int_0^\infty \mathrm{d}\tau\, \dot{f}_{t-\tau}^\alpha \dot{\chi}_\tau^{\rho\rho}\right) \stackrel{!}{=} -\sum_{\alpha\neq\rho} F^\alpha \left(\dot{\chi}_0^{\rho\alpha} f_t^\alpha - \int_0^\infty \mathrm{d}\tau\, \dot{f}_{t-\tau}^\alpha \dot{\chi}_\tau^{\rho\alpha}\right). \tag{4.21}$$

The second step follows from the observation that Equation (4.21) is linear in the driving fields. Therefore, instead of making an attempt at solving the integro-differential equation in (4.21) directly, the condition can promptly be solved for the chemical protocol in Fourier space with simple algebraic means. Decomposing the protocols again into Fourier series and using the Fourier transform (4.18), the Fourier modes can be decoupled from one another, and the self-consistency condition reduces to an algebraic equation for the expansion coefficients:

$$c_k^\rho \stackrel{!}{=} \sum_{\alpha\neq\rho} \left[-\frac{(\dot\chi_0^{\rho\alpha} - \mathrm{i}k\Omega\tilde\chi_k^{\rho\alpha})}{(\dot\chi_0^{\rho\rho} - \mathrm{i}k\Omega\tilde\chi_k^{\rho\rho})} \right] \frac{F^\alpha}{F^\rho} c_k^\alpha. \tag{4.22}$$

This mean-field type result makes it possible to describe systems with, on average, conserved particle numbers within the grand-canonical framework, which is considerably simpler on a technical level than the canonical ensemble [46]. The result in (4.22) demonstrates that the chemical driving fields f_t^ρ for these effectively canonical systems are fully determined by the thermal f_t^q and mechanical f_t^w protocols and the self-consistency condition $J_t^\rho = 0$.

The thermodynamic performance of a heat engine is characterized by two figures of merit, the net periodic power $P = -TF^wJ^w$ and efficiency $\eta \equiv P/J^q$, and they are determined by the Onsager coefficients and the thermodynamic forces [36]. As a consequence of the self-consistency condition (4.22), the Onsager coefficients depend only on the thermal and mechanical driving fields and not on the chemical potential:

$$J^\alpha = \sum_{\beta=q,w} \mathcal{L}^{\alpha\beta}F^\beta \quad \text{with} \quad \mathcal{L}^{\alpha\beta} \equiv \sum_{k=-\infty}^{\infty} \mathrm{i}\Omega k c_{-k}^\alpha \left[\tilde\chi_k^{\alpha\rho} \frac{(\dot\chi_0^{\rho\alpha} - \mathrm{i}k\Omega\tilde\chi_k^{\rho\alpha})}{(\dot\chi_0^{\rho\rho} - \mathrm{i}k\Omega\tilde\chi_k^{\rho\rho})} - \tilde\chi_k^{\alpha\beta} \right] c_k^\beta. \tag{4.23}$$

Here, $\mathcal{L}^{\alpha\beta}$ denote effective Onsager coefficients for systems with, on average, conserved particle numbers. In terms of these coefficients, the thermodynamic figures of merit assume the expressions

$$P = -TF^w\left(\mathcal{L}^{wq}F^q + \mathcal{L}^{ww}F^w\right) \quad \text{and} \quad \eta = -TF^w \frac{\mathcal{L}^{ww}F^w + \mathcal{L}^{wq}F^q}{\mathcal{L}^{qw}F^w + \mathcal{L}^{qq}F^q}. \tag{4.24}$$

4.4 Bosonic systems in harmonic potentials

The simplicity of linear response lies in that the response functions depend only on equilibrium quantities [36]. As such, we can draw heavily upon the results and methods of Chapter 2, specifically grand-canonical thermostatistics and the integral approximation, to give $\chi_t^{\alpha\beta}$ explicit expressions. Also, the base chemical potential is naturally chosen to fix the mean particle number of trapped bosons according to (2.5).

4.4.1 Perturbation operators

We now work exclusively with harmonically trapped two-dimensional gases, described by the time-dependent many-body Hamiltonian

$$\begin{aligned} H_t =& \sum_{\mathbf{n}} \hbar\omega(n+1) A^\dagger_{\mathbf{n}} A_{\mathbf{n}} + \sum_{\mathbf{mn}} \langle \mathbf{m}| \frac{1}{2} m\hat{\omega}_t^2 \mathbf{x}^2 |\mathbf{n}\rangle A^\dagger_{\mathbf{m}} A_{\mathbf{n}} \\ =& H + \sum_{\mathbf{mn}} \frac{\hbar\hat{\omega}^2}{2\omega} \left(\frac{\hat{\omega}_t}{\hat{\omega}}\right)^2 \frac{1}{2} \langle \mathbf{m}| (\mathbf{a}+\mathbf{a}^\dagger)^2 |\mathbf{n}\rangle A^\dagger_{\mathbf{m}} A_{\mathbf{n}} \equiv H + \Delta H f_t^w g^w, \end{aligned} \tag{4.25}$$

where $\hat{\omega}_t$ is a time-dependent modulation with the maximum value $\hat{\omega}$, $\Delta H \equiv \hbar\hat{\omega}^2/2\omega$, $f_t^w \equiv (\hat{\omega}_t/\hat{\omega})^2$ the mechanical driving field with values between 0 and 1, and

$$\begin{aligned} g^w \equiv& \sum_{\mathbf{n}} (n+1) A^\dagger_{\mathbf{n}} A_{\mathbf{n}} + \frac{1}{2} \sum_{\nu=x,y} \sqrt{(n_\nu+1)(n_\nu+2)} \left(A^\dagger_{\mathbf{n}^+_\nu} A_{\mathbf{n}} + A^\dagger_{\mathbf{n}} A_{\mathbf{n}^+_\nu} \right) \\ \equiv& g^w_{\text{cl.}} + g^w_{\text{qu.}} \end{aligned} \tag{4.26}$$

the mechanical perturbation operator. Also, we have introduced the shorthand notation $\mathbf{n}^+_\nu \equiv \mathbf{n} + 2\mathbf{e}_\nu$ with $\mathbf{e}_x \equiv (1,0)$ and $\mathbf{e}_y \equiv (0,1)$. The first term $g^w_{\text{cl.}}$ can be considered quasi-classical as it commutes with the unperturbed Hamiltonian H, while the second term $g^w_{\text{qu.}}$ is the quantum correction term that accounts for coherences between the eigenstates of the unperturbed Hamiltonian [36]. The free dynamics of the many-particle system is governed by the Lindblad equation $\dot{\varrho}_t = \hat{\mathsf{L}}_t \varrho_t$ [28], where

$$\begin{aligned} \hat{\mathsf{L}}_t \bullet =& -\frac{i}{\hbar}[H_t, \bullet] + \sum_{\mathbf{n}} \gamma_{\mathbf{n}} \left(A_{\mathbf{n}} \bullet A^\dagger_{\mathbf{n}} - \frac{1}{2}\{\bullet, A^\dagger_{\mathbf{n}} A_{\mathbf{n}}\} \right) \\ &+ \gamma^\dagger_{\mathbf{n}} \left(A^\dagger_{\mathbf{n}} \bullet A_{\mathbf{n}} - \frac{1}{2}\{\bullet, A_{\mathbf{n}} A^\dagger_{\mathbf{n}}\} \right) \end{aligned} \tag{4.27}$$

denotes the many-body generator. Its time-reversed adjoint is $\hat{\mathsf{L}}^\ddagger_t \equiv \hat{\mathsf{H}}_t + \hat{\mathsf{D}}^\dagger$, where the adjoint dissipator reads [36]

$$\hat{\mathsf{D}}^\dagger \bullet \equiv \sum_{\mathbf{n}} \gamma_{\mathbf{n}} \left(A^\dagger_{\mathbf{n}} \bullet A_{\mathbf{n}} - \frac{1}{2}\{\bullet, A^\dagger_{\mathbf{n}} A_{\mathbf{n}}\} \right) + \gamma^\dagger_{\mathbf{n}} \left(A_{\mathbf{n}} \bullet A^\dagger_{\mathbf{n}} - \frac{1}{2}\{\bullet, A_{\mathbf{n}} A^\dagger_{\mathbf{n}}\} \right). \tag{4.28}$$

The linear-response functions involve exponentials of the unperturbed superoperator $\hat{\mathsf{L}}^\ddagger \equiv \hat{\mathsf{L}}^\ddagger_t|_{\Delta H=0}$ acting on the perturbation operators δg^α. The action of this unperturbed superoperator on $A^\dagger_{\mathbf{m}} A_{\mathbf{n}}$ can be evaluated by applying the bosonic commutation relation repeatedly to the definition of the adjoint dissipator. The resulting expression

$$\hat{\mathsf{L}}^\ddagger A^\dagger_{\mathbf{m}} A_{\mathbf{n}} = (-\Gamma + \mathrm{i}\omega(m-n))\, \delta(A^\dagger_{\mathbf{m}} A_{\mathbf{n}}) \tag{4.29}$$

implies the identities

$$e^{\hat{\mathsf{L}}^\ddagger t}\delta g^\rho = -\sum_{\mathbf{n}} e^{-\Gamma t}\delta(A^\dagger_{\mathbf{n}}A_{\mathbf{n}}) = e^{-\Gamma t}\delta g^\rho, \tag{4.30}$$

$$e^{\hat{\mathsf{L}}^\ddagger t}\delta g^q = -\sum_{\mathbf{n}} e^{-\Gamma t}\xi_{\mathbf{n}}\delta(A^\dagger_{\mathbf{n}}A_{\mathbf{n}}) = e^{-\Gamma t}\delta g^q, \tag{4.31}$$

$$\begin{aligned} e^{\hat{\mathsf{L}}^\ddagger t}\delta g^w = &\sum_{\mathbf{n}} e^{-\Gamma t}\Big[(n+1)\delta(A^\dagger_{\mathbf{n}}A_{\mathbf{n}}) \\ &+ \frac{1}{2}\sum_{\nu=x,y}\sqrt{(n_\nu+1)(n_\nu+2)}\left(e^{\mathrm{i}2\omega t}A^\dagger_{\mathbf{n}^+_\nu}A_{\mathbf{n}} + e^{-\mathrm{i}2\omega t}A^\dagger_{\mathbf{n}}A_{\mathbf{n}^+_\nu}\right)\Big]. \end{aligned} \tag{4.32}$$

These follow from the identity operator being an eigenvector of the adjoint generator with the eigenvalue zero [36]. Here, we have fixed the net rates $\Gamma \equiv \gamma_{\mathbf{n}} - \gamma^\dagger_{\mathbf{n}}$ for the eigenstates $|\mathbf{n}\rangle$ by parameterizing

$$\gamma_n = \frac{\Gamma}{1-e^{-\xi_{\mathbf{n}}/T}} \quad \text{and} \quad \gamma^\dagger_n = \frac{\Gamma}{e^{\xi_{\mathbf{n}}/T}-1} \quad \text{so that} \quad \gamma_{\mathbf{n}} - \gamma^\dagger_{\mathbf{n}} = \Gamma, \tag{4.33}$$

which satisfies the detailed-balance condition.

4.4.2 Linear-response functions

We are now ready to evaluate the response functions

$$\chi^{\alpha\beta}_t = \langle\!\langle g^\alpha, e^{\hat{\mathsf{L}}^\ddagger t}g^\beta\rangle\!\rangle = \int_0^1 \mathrm{d}s\,\langle\delta g^\alpha R^s(e^{\hat{\mathsf{L}}^\ddagger t}\delta g^\beta)R^{-s}\rangle.$$

Using that the perturbation operators δg^q and δg^ρ as well as the quasi-classical contribution $\delta g^w_{\text{cl.}}$ to the mechanical perturbation in (4.26) commute with the thermal state and that the quantum correction $g^w_{\text{qu.}}$ in (4.26) does not contribute to the Kubo brackets with δg^q or δg^ρ due to its purely non-diagonal structure with respect to the joint eigenbasis of H, g^ρ, g^q and $g^w_{\text{cl.}}$, the time-independent parts of all responses but χ^{ww}_t can be expressed entirely in terms of covariances $\langle g^\alpha g^\beta\rangle - \langle g^\alpha\rangle\langle g^\beta\rangle$. Since

$$\langle A^\dagger_{\mathbf{m}}A_{\mathbf{m}}A^\dagger_{\mathbf{n}}A_{\mathbf{n}}\rangle = \begin{cases} 2\langle A^\dagger_{\mathbf{n}}A_{\mathbf{n}}\rangle^2 + \langle A^\dagger_{\mathbf{n}}A_{\mathbf{n}}\rangle & \text{for} \quad \mathbf{m}=\mathbf{n} \\ \langle A^\dagger_{\mathbf{m}}A_{\mathbf{m}}\rangle\langle A^\dagger_{\mathbf{n}}A_{\mathbf{n}}\rangle & \text{for} \quad \mathbf{m}\neq\mathbf{n}, \end{cases} \tag{4.34}$$

we are left with the response functions

$$\chi^{\alpha\beta}_t = \sum_{n=0}^{\infty} g_n D^\alpha_n D^\beta_n \mathfrak{n}_n(\mathfrak{n}_n+1)e^{-\Gamma t} + g_n C^{\alpha\beta}_n \mathfrak{n}_{n+2}(\mathfrak{n}_n+1)e^{-\Gamma t}\cos(2\omega t), \tag{4.35}$$

where the coefficients D^α_n and $C^{\alpha\beta}_n$ are defined as

$$D^\rho_n \equiv 1,\ D^q_n \equiv \xi_n = \hbar\omega n - \mu,\ D^w_n \equiv -n-1,\ C^{\alpha\beta}_n \equiv \frac{(n^2+6n+8)\delta_{ww,\alpha\beta}}{\operatorname{csch}(\hbar\omega/T)e^{-\hbar\omega/T}\hbar\omega/T}. \tag{4.36}$$

The sums in the response functions do not admit analytic expressions, but we can replace the sums with integrals as we did in Chapter 2 if $T \gg \hbar\omega$ [25]. Thus, we can write the integrated response functions in the form

$$\chi_t^{\alpha\beta} \simeq \mathcal{D}^{\alpha\beta} e^{-\Gamma t} + \mathcal{C}^{\alpha\beta} e^{-\Gamma t} \cos(2\omega t), \tag{4.37}$$

where the oscillatory component is a result of coherence, or in Fourier space as

$$\tilde{\chi}_k^{\alpha\beta} \simeq -\mathcal{D}^{\alpha\beta} \frac{\Gamma}{\Gamma + \mathrm{i}k\Omega} - \mathcal{C}^{\alpha\beta} \frac{\Gamma^2 + 4\omega^2 + \mathrm{i}k\Omega}{4\omega^2 + (\Gamma + \mathrm{i}k\Omega)^2}, \tag{4.38}$$

where we have introduced the integrated coefficients

$$\begin{aligned} \mathcal{D}^{\alpha\beta} &\equiv g_0 D_0^\alpha D_0^\beta \mathfrak{n}_0(\mathfrak{n}_0 + 1) + \int_0^\infty \mathrm{d}n\, g_n D_n^\alpha D_n^\beta \mathfrak{n}_n(\mathfrak{n}_n + 1), \\ \mathcal{C}^{\alpha\beta} &\equiv g_0 C_0^{\alpha\beta} \mathfrak{n}_2(\mathfrak{n}_0 + 1) + \int_0^\infty \mathrm{d}n\, g_n C_n^{\alpha\beta} \mathfrak{n}_{n+2}(\mathfrak{n}_n + 1). \end{aligned} \tag{4.39}$$

The coefficients $\mathcal{D}^{\alpha\beta}$ can be expressed in terms of n-weighted integrals over the particle number fluctuations

$$\int_0^\infty \mathrm{d}n\, n^s \mathfrak{n}_n(\mathfrak{n}_n + 1) = s! \left(\frac{T}{\hbar\omega}\right)^{s+1} \mathrm{Li}_s(z), \tag{4.40}$$

where s is a non-negative integer, while the coefficient $\mathcal{C}^{\alpha\beta}$ depends on the integral

$$\int_0^\infty \mathrm{d}n\, n^s \mathfrak{n}_{n+2}(\mathfrak{n}_n + 1) = s! \left(\frac{T}{\hbar\omega}\right)^{s+1} \frac{\mathrm{Li}_{s+1}(z) - \mathrm{Li}_{s+1}(ze^{-2\hbar\omega/T})}{e^{2\hbar\omega/T} - 1}, \tag{4.41}$$

which is evaluated with the partial fraction decomposition by breaking $\mathfrak{n}_{n+2}(\mathfrak{n}_n + 1) = (\mathfrak{n}_n - \mathfrak{n}_{n+2})/(e^{2\hbar\omega/T} - 1)$ into a linear combination of Bose-Einstein factors. The full expressions for the integrated coefficients $\mathcal{C}^{\alpha\beta}$, $\mathcal{D}^{\alpha\beta}$ can be found in Appendix B.

4.4.3 Fluxes

The Onsager coefficients $L^{\alpha\beta} = L^{\alpha\beta}[f_t^\alpha, f_t^\beta]$ are quadratic functionals of the periodic driving protocols, which can be expanded into Fourier series. These expansion coefficients as well as the response functions fully determine the linear-response thermodynamics of the bosonic system [36]. The generalized heat and work-generating fluxes can be then written in a particle-conserving form:

$$\begin{aligned} J^\alpha = \sum_{\beta=q,w} \sum_{k=1}^{\infty} \Bigg[&\left(\mathcal{D}^{\alpha\beta} - \frac{\mathcal{D}^{\alpha\rho}\mathcal{D}^{\rho\beta}}{\mathcal{D}^{\rho\rho}}\right) \frac{2\Gamma\Omega^2 k^2 c_k^{\alpha *} c_k^\beta}{\Gamma^2 + k^2\Omega^2} \\ &+ \mathcal{C}^{\alpha\beta} \frac{2\Gamma\Omega^2 k^2 (\Gamma^2 + 4\omega^2 + k^2\Omega^2) c_k^{\alpha *} c_k^\beta}{(\Gamma^2 + 4\omega^2)^2 + 2k^2(\Gamma^2 - 4\omega^2)\Omega^2 + k^4\Omega^4} \Bigg] F^\beta. \end{aligned} \tag{4.42}$$

The result (4.42) is general and can be applied to any particle-conserving system. Whether the infinite sums in (4.42) admit analytic expressions or not is, of course, determined by the expansion coefficients of the driving fields.

4.5 Finite-time thermodynamics of Otto cycles

We will now apply the developed linear-response formalism to study the finite-time Otto cycle. The cycle is characterized by sudden changes in temperature and trap strength, induced by in-phase, periodic extensions of the step-like thermal and mechanical driving fields, which are represented by the same Fourier decomposition

$$f_t = \sum_{k=-\infty}^{\infty} c_k e^{\mathrm{i}k\Omega t}, \quad \text{where} \quad c_k = \frac{1-e^{-\mathrm{i}k\Omega\tau}}{\mathrm{i}2\pi k} \quad \Rightarrow \quad |c_k|^2 = \frac{1-\cos(k\Omega\tau)}{2\pi^2 k^2}, \tag{4.43}$$

with amplitudes ΔT and $\Delta\omega$. The instantaneous parameter switches happen at $t = 0$ and $t = \tau$ modulo $\mathcal{T}$. Although τ can be chosen arbitrarily, it is convenient to choose $\tau = \mathcal{T}/2$ as it not only leads to elegant expressions but also extremizes the thermodynamic fluxes in Equation (4.42).

The external driving fields being represented by the same protocol f_t is a feature specific to the Otto cycle and allows for the double sum in (4.42) to be separated into a product of sums. In the previous section, we showed that the individual contributions to linear-response functions separate into time-dependent and time-independent parts in time-domain, and this property is preserved by the Fourier transform (4.18) due to linearity. Therefore, the sums in Equation (4.42) can be evaluated by noting that

$$\sum_{k=1}^{\infty} \frac{2\Gamma\Omega^2 k^2 |c_k|^2}{\Gamma^2 + k^2\Omega^2} = \frac{1}{\mathcal{T}} \tanh\left(\frac{\Gamma\mathcal{T}}{4}\right), \tag{4.44}$$

$$\sum_{k=1}^{\infty} \frac{2\Gamma\Omega^2 k^2 |c_k|^2 (\Gamma^2 + 4\omega^2 + k^2\Omega^2)}{(\Gamma^2 + 4\omega^2)^2 + 2k^2(\Gamma^2 - 4\omega^2)\Omega^2 + k^4\Omega^4} = \frac{1}{2\mathcal{T}} \sum_{s=\pm 1} \tanh\left(\frac{(\Gamma + s\cdot \mathrm{i}2\omega)\mathcal{T}}{4}\right). \tag{4.45}$$

The sum of hyperbolic tangents in (4.46) has the alternative expression

$$\frac{1}{2}\sum_{s=\pm 1} \tanh\left(\frac{(\Gamma + s\cdot \mathrm{i}2\omega)\mathcal{T}}{4}\right) = \frac{\sinh(\Gamma\mathcal{T}/2)}{\cosh(\Gamma\mathcal{T}/2) + \cos(\pi\cdot 2\omega/\Omega)}, \tag{4.46}$$

which follows from basic identities for hyperbolic functions and complex numbers [42]. Substituting these results into the particle-conserving fluxes reduces the final expressions to just

$$\begin{aligned} J^\alpha = \frac{1}{\mathcal{T}} \sum_{\beta=q,w} \Bigg[&\left(\mathcal{D}^{\alpha\beta} - \frac{\mathcal{D}^{\alpha\rho}\mathcal{D}^{\rho\beta}}{\mathcal{D}^{\rho\rho}}\right) \tanh\left(\frac{\Gamma\mathcal{T}}{4}\right) \\ &+ \mathcal{C}^{\alpha\beta}\left(\frac{\sinh(\Gamma\mathcal{T}/2)}{\cosh(\Gamma\mathcal{T}/2) + \cos(\pi\cdot 2\omega/\Omega)}\right)\Bigg] F^\beta. \end{aligned} \tag{4.47}$$

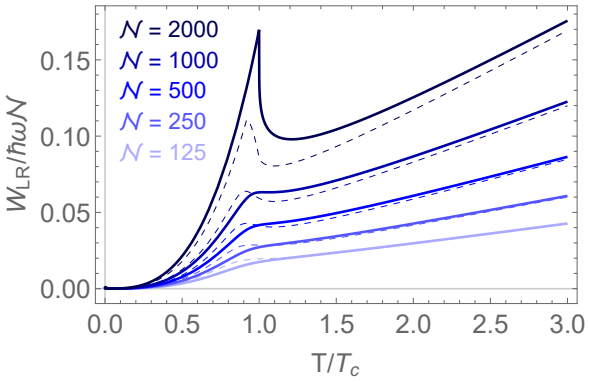

Figure 4.1: Work in the linear-response regime against T/T_c. The solid lines depict the average periodic work per particle in the linear-response regime with the results of Chapter 2, derived with thermostatistics, represented by the dashed lines. Again, we have fixed $\Delta T/T = 1/10$ and $\Delta\omega/\omega = 1/100$.

4.5.1 Performance in the long-cycle limit

In the long-cycle limit $\mathcal{T} \to \infty$, the results for the ideal Otto engines considered in Chapter 2 can be used as a consistency check for the linear-response calculations. In this limit, the coherence-induced cosine term in (4.47) is suppressed by the hyperbolic functions, meaning that coherence has no effect on performance at long periods. The linear-response power and work are given by [36]

$$P_{\rm LR}(\mathcal{T}) \equiv -TF^w J^w|_{\mathcal{T}} \qquad \text{and} \qquad W_{\rm LR}(\mathcal{T}) \equiv \mathcal{T} P_{\rm LR}(\mathcal{T}), \tag{4.48}$$

and the cyclic work in the long-time limit, $W_{\rm LR} \equiv \lim_{\mathcal{T}\to\infty}\{-\mathcal{T}TF^w J^w|_{\mathcal{T}}\}$, is plotted against temperature in Figure 4.1. When the base temperature T is below the critical value, the linear-response work becomes a cubic function of temperature, thus mimicking the earlier results for ideal Otto cycles, while at high temperatures the linear-response work function settles into a linear limit as per semiclassical statistics. Therefore, in the cubic- and linear-growth regimes of power, where the working fluid does not undergo a phase transition during the cycle, the linear response theory is able to describe the thermodynamic performance of the Otto engine quite accurately. Also, the theory predicts a sudden transition from one regime to another. Overall, linear response captures the qualitative behavior of the exact plots from Chapter 2.

Here, the main limitation of linear response is its inability to predict the phase-transition regime, where the system undergoes condensation and evaporation during the cycle, which boosts the periodic power. Instead, linear response is only able to describe the cubic- and linear-growth regimes of power and predicts that the engine transitions from one to the other as soon as the base temperature crosses the critical value. This shortcoming is not completely unexpected, since linear response relies on the analytic behavior of equilibrium quantities under the variation of external driving

parameters. In a two-dimensional harmonic potential, the chemical potential of a Bose gas behaves non-analytically at the condensation temperature, leading to the observed changes in the expected behavior of the linear-response thermodynamics at long period lengths. As a consequence of the phase-transition regime going unobserved and with the work function either plateauing or developing a pronounced kink near the critical temperature, the root cause of the power enhancement, the considerable differences in the ground-state population induced by the phase transition, is not properly captured by the linear response theory.

4.5.2 Finite-time effects and coherence

In Figure 4.2, we show the behavior of the work and power outputs, which we have normalized by $\hbar\omega\mathcal{N}$ and $\hbar\omega\Gamma\mathcal{N}$ respectively, against period length and the ratio of the oscillation frequency to the driving frequency. Note that the normalization removes the linear scaling of work and power in ω from the figures, leaving only the oscillations visible. Taken together, the subfigures of 4.2 demonstrate the effects of quantum coherence under finite-time driving. The semiclassical limit, where the energy eigenstates form a continuum as the gap $\hbar\omega$ between adjacent eigenstates becomes negligibly small, is represented by the ratio $2\omega/\Omega = 0$ between the frequency of coherent oscillations and the driving frequency. In this limit, the quantum correction $g^w_{\text{qu.}}$ to mechanical perturbation in Equation (4.26) assumes an approximately diagonal form in the eigenstates of the unperturbed Hamiltonian and the integral in Equation (4.41), which can be identified as a q-derivative [50], reduces to the integral in Equation (4.40). Physically, this is equivalent to the system's response to periodic driving decaying so fast that the coherent oscillations in χ^{ww}_t, defined in (4.37), have no effect on the thermodynamics. In this semiclassical limit, where $2\omega/\Omega \simeq 0$, the work increases rapidly as a function of period length until suddenly settling into a constant value, which is typical behavior of the hyperbolic tangents dominating the time-dependence of the canonical fluxes. As the work assumes a constant value, the average power becomes an inversely varying function of the period length that can be amplified by driving the system faster.

Coherent effects become observable in fast driven systems, where their magnitude is determined by the ratio $2\omega/\Omega$ in a periodic manner. As the trap is stiffened from the semiclassical limit $\omega \simeq 0$, the contribution of the only phenomenological coefficient dependent on the quantum correction $g^w_{\text{qu.}}$, L^{ww}, begins to impair the performance as resonant dips in power develop when the system is driven at the oscillation frequency. Due to periodicity, the semiclassical performance is recovered in the quantum regime at even integer ratios $2\omega/\Omega$ but never overcome. This result suggests coherent effects cannot be harnessed to overcome semiclassical bounds on performance as they only diminish the performance of quantum many-particle Otto engines in the linear-response regime, although Figure 4.2 indicates it can shift the power maximum, which is normally found at infinitely fast cycles, since more power can be extracted from a coherent system so long as the period is kept short enough for the system not to decohere.

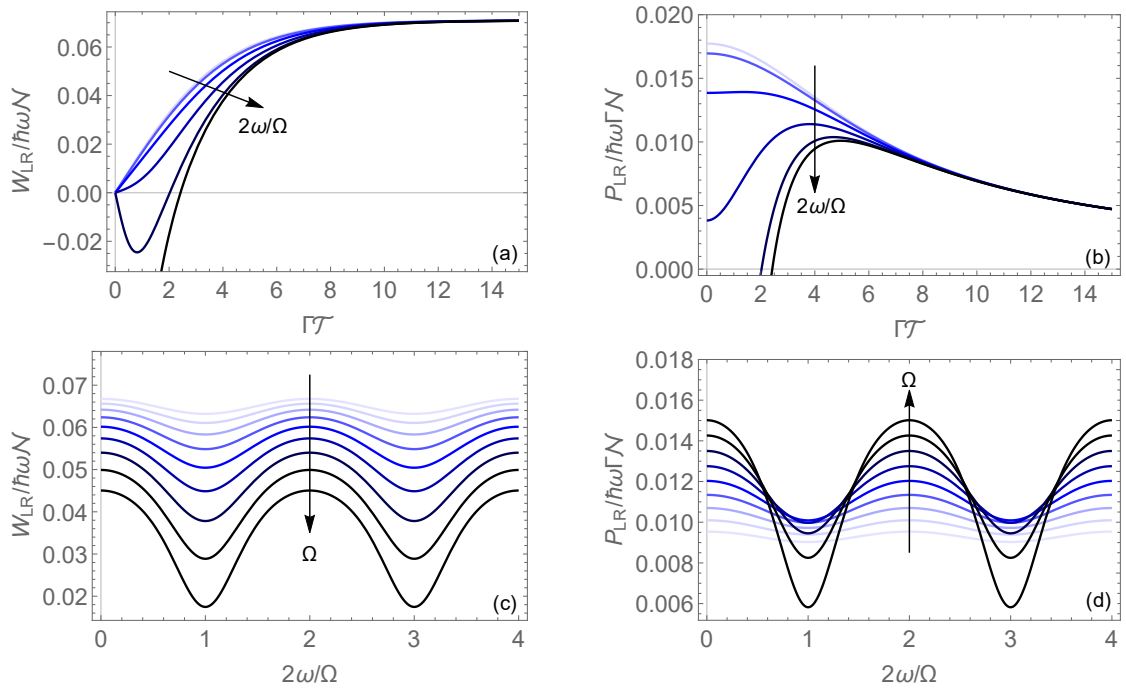

Figure 4.2: Time-dependence of **(a)** work and **(b)** power, normalized by $\hbar\omega\mathcal{N}$ and $\hbar\omega\Gamma\mathcal{N}$, as well as the effect of coherent oscillations on **(c)** work and **(d)** power in the linear-response regime. From **(a)** and **(c)**, we see that even small changes in period length have a noticeable effect on the work output at short period lengths where performance is diminished by the effects of coherence, determined by the ratio $2\omega/\Omega$, but also that the periodic net work settles into a constant value at longer periods where coherence has no effect on performance. Consequently, the periodic power, depicted in **(b)** and **(d)**, develops into an inversely proportional function of $\mathcal{T}$ at long period lengths, where coherence has no impact on performance; at short cycles, on the other hand, coherence can shift the power maximum from $\mathcal{T} = 0$, as short cycles are preferred in the absence of coherence, to finite values. Here, we have set $T/T_c = 0.95$ and fixed $\Delta T/T = 1/10$ with $\mathcal{N} = 1000$ and Γ set to unity, but the qualitative behavior seen in the subfigures is also reproduced at other temperatures and mean particle numbers. Here, $(2\omega/\Omega)/(\pi/5)$ assumes values $k \in \{0, 1, \ldots, 5\}$ in **(a)** and **(b)** and Ω/Γ values $k \in \{3, 4, \ldots, 7\}$ in **(c)** and **(d)**.

Chapter 5

Mean-field dynamics

Although enforcing the self-consistency condition (4.22) allows for the study of particle-conserving systems using the grand-canonical ensemble, linear response is limited to weakly driven systems [36, 49]. To extend the master equation approach to any periodically driven system with Lindblad dynamics, an alternative formulation for finite-time thermodynamics can be derived by considering the first law and the time-evolution of the internal energy within a mean-field type framework.

In periodically modulated systems coupled to thermochemical reservoirs, the internal energy changes due to the energy eigenstates and their populations evolving in time. If the coupling between the system and the reservoir is weak, the Lindblad generator introduced earlier can be used to derive equations of motion for the generalized occupations $\mathsf{N}_{\mathbf{mn},t} \equiv \mathsf{N}_{\mathbf{mn}} \equiv \mathrm{Tr}\{A^{\dagger}_{\mathbf{m},t} A_{\mathbf{n},t} \varrho_t\}$. Note that we routinely omit the explicit notation for the time-dependence of these mean-field variables throughout this chapter. The resulting mean-field equations of motion allow for the finite-time thermodynamics of heat engines to be studied exactly within the Lindblad framework without solving the master equation even approximately.

Unfortunately, due to the grand-canonical structure of the Lindblad generator, the particle number is not identically conserved by the occupation equations of motion. Therefore, a numerical routine must be developed for constructing a particle-conserving chemical potential protocol in a piecewise manner by extrapolation. Due to the high amount of computational resources required for accuracy comparable to the linear response theory, it is not our objective to perform extensive simulations but to present an outline of the general method and demonstrate its ability to maintain the fixed total particle number in quantum Otto engines.

5.1 Equations of motion

Starting from the first law $\dot{E}_t = J_t^E - P_t$, we note that latter two quantities can be written as instantaneous ensemble averages

$$J_t^E = \mathrm{Tr}\{H_t \dot{\varrho}_t\} = \mathrm{Tr}\{H_t \hat{\mathsf{D}}_t \varrho_t\} = \mathrm{Tr}\{(\hat{\mathsf{D}}_t^\dagger H_t)\varrho_t\} \quad \text{and} \quad P_t = \mathrm{Tr}\{\dot{H}_t \varrho_t\}. \tag{5.1}$$

In the weak-coupling regime, it can be shown with bosonic commutation relations that the ensemble averages $\mathsf{N}_{\mathbf{mn}} \equiv \mathrm{Tr}\{A_{\mathbf{m},t}^\dagger A_{\mathbf{n},t} \varrho_t\}$, where the diagonal $\mathbf{m} = \mathbf{n}$ elements represent instantaneous occupation numbers and the off-diagonals $\mathbf{m} \neq \mathbf{n}$ coherence between different eigenstates, evolve in time according to

$$\begin{aligned} \dot{\mathsf{N}}_{\mathbf{mn}} &= \mathrm{Tr}\{A_{\mathbf{m},t}^\dagger A_{\mathbf{n},t} \hat{\mathsf{L}}_t \varrho_t\} + \mathrm{Tr}\{(\dot{A}_{\mathbf{m},t}^\dagger A_{\mathbf{n},t} + A_{\mathbf{m},t}^\dagger \dot{A}_{\mathbf{n},t})\varrho_t\} \\ &= \mathrm{Tr}\{\hat{\mathsf{K}}_t (A_{\mathbf{m},t}^\dagger A_{\mathbf{n},t})\varrho_t\} + \mathrm{Tr}\{(\dot{A}_{\mathbf{m},t}^\dagger A_{\mathbf{n},t} + A_{\mathbf{m},t}^\dagger \dot{A}_{\mathbf{n},t})\varrho_t\} \equiv \mathsf{N}_{\mathbf{mn}}^{\text{diss.}} + \mathsf{N}_{\mathbf{mn}}^{\text{coh.}}, \end{aligned} \tag{5.2}$$

where $\hat{\mathsf{K}}_t \equiv -\hat{\mathsf{H}}_t + \hat{\mathsf{D}}_t^\dagger$ denotes the generator of the operator equations of motion in the Heisenberg picture. The Liouvillian superoperator $\hat{\mathsf{H}}_t$ can be ignored in Equation (5.2) for the diagonal elements $\mathsf{N}_{\mathbf{nn}}$, as the number operators $A_{\mathbf{n},t}^\dagger A_{\mathbf{n},t}$ belong to the null space of the Liouvillian superoperator $\hat{\mathsf{H}}_t$. Using these generalized occupations, we can derive expressions for the average periodic energy uptake and power by averaging J_t^E and P_t over a period in the cyclic limit for

$$J^E = + \lim_{t\to\infty} \frac{1}{\mathcal{T}} \int_t^{t+\mathcal{T}} \mathrm{d}s \sum_{\mathbf{n}} \left[\hbar\omega_s (n+1) \dot{\mathsf{N}}_{\mathbf{nn},s}^{\text{diss.}} \right], \tag{5.3}$$

$$P = - \lim_{t\to\infty} \frac{1}{\mathcal{T}} \int_t^{t+\mathcal{T}} \mathrm{d}s \sum_{\mathbf{n}} \left[\hbar\dot{\omega}_s (n+1) \mathsf{N}_{\mathbf{nn},s} + \hbar\omega_s (n+1) \dot{\mathsf{N}}_{\mathbf{nn},s}^{\text{coh.}} \right]. \tag{5.4}$$

Here, the first contribution to the average power in (5.4) is the quasi-classical contribution from the periodic modulation of the energy levels, while the second contribution represents the effects of coherence.

5.1.1 Dissipation-induced terms

The first contributions to the equations of motion $\dot{\mathsf{N}}_{\mathbf{mn},t}^{\text{diss.}}$, describing dissipative losses, are always present in systems with Lindblad dynamics. By plugging in the definition of the adjoint dissipator from (3.4) and using the bosonic commutation relations to break down the operator strings into pairs, we arrive at the equations

$$\begin{aligned} \dot{\mathsf{N}}_{\mathbf{mn}}^{\text{diss.}} &= (-\Gamma + \mathrm{i}\omega_t(m-n)) \left(\mathsf{N}_{\mathbf{mn}} - \frac{\delta_{\mathbf{mn}}}{e^{(\varepsilon_{\mathbf{n},t} - \mu_t)/T_t} - 1} \right) \\ &= (-\Gamma + \mathrm{i}\omega_t(m-n)) \left(\mathsf{N}_{\mathbf{mn}} - \bar{\mathsf{N}}_{\mathbf{mn}} \right). \end{aligned} \tag{5.5}$$

Here, we have parameterized the transition rates according to (4.33), meaning that the detailed-balance condition is satisfied. Also, $\bar{\mathsf{N}}_{\mathbf{mn}} \equiv \mathrm{Tr}\{A^\dagger_{\mathbf{m},t} A_{\mathbf{n},t} R_t\}$ denotes the average of $A^\dagger_{\mathbf{m},t} A_{\mathbf{n},t}$ with respect to the instantaneous equilibrium state. Equation (5.5) implies that the generalized occupations are constantly evolving towards the instantaneous equilibrium populations.

5.1.2 Coherence-induced terms

To evaluate the time derivatives of the Fock operators for the second contributions $\dot{\mathsf{N}}^{\mathrm{coh.}}_{\mathbf{mn}}$, which are induced by periodic modulations of the trap strength, we perform a change of basis [40] to a time-independent basis and another transformation back to the time-dependent one:

$$\dot{A}^\dagger_{\mathbf{l},t} = \sum_{\boldsymbol{\lambda}} A^\dagger_{\boldsymbol{\lambda}} \langle \boldsymbol{\lambda} | \dot{\mathbf{l}}_t \rangle = \sum_{\mathbf{k}\boldsymbol{\lambda}} A^\dagger_{\mathbf{k},t} \langle \mathbf{k}_t | \boldsymbol{\lambda} \rangle \langle \boldsymbol{\lambda} | \dot{\mathbf{l}}_t \rangle = \sum_{\mathbf{k}} A^\dagger_{\mathbf{k},t} \langle \mathbf{k}_t | \dot{\mathbf{l}}_t \rangle. \tag{5.6}$$

The overlap can be found by differentiating the instantaneous Schrödinger equation for $|\mathbf{l}_t\rangle$ and projecting it onto $|\mathbf{k}_t\rangle$. The end result is

$$\dot{A}^\dagger_{\mathbf{l},t} = \frac{\dot{\omega}_t}{4\omega_t} \sum_{\nu=x,y} \left(\sqrt{l_\nu (l_\nu - 1)} A^\dagger_{\mathbf{l}^-_\nu,t} - \sqrt{(l_\nu + 1)(l_\nu + 2)} A^\dagger_{\mathbf{l}^+_\nu,t} \right), \tag{5.7}$$

where we have denoted $\mathbf{e}_x \equiv (1,0)$, $\mathbf{e}_y \equiv (0,1)$ and $\mathbf{l}^\pm_\nu \equiv \mathbf{l} \pm 2\mathbf{e}_\nu$, leading to

$$\begin{aligned} \dot{\mathsf{N}}^{\mathrm{coh.}}_{\mathbf{mn}} = \frac{\dot{\omega}_t}{4\omega_t} \sum_{\nu=x,y} \Bigg(& \sqrt{m_\nu (m_\nu - 1)} \mathsf{N}_{\mathbf{m}^-_\nu \mathbf{n}} - \sqrt{(m_\nu + 1)(m_\nu + 2)} \mathsf{N}_{\mathbf{m}^+_\nu \mathbf{n}} \\ & + \sqrt{n_\nu (n_\nu - 1)} \mathsf{N}_{\mathbf{m}\mathbf{n}^-_\nu} - \sqrt{(n_\nu + 1)(n_\nu + 2)} \mathsf{N}_{\mathbf{m}\mathbf{n}^+_\nu} \Bigg). \end{aligned} \tag{5.8}$$

Thus, periodic modulations of the trap strength couple the mean occupations with the even off-diagonal coherence terms. The generalized occupations can then be used to express the thermodynamic quantities of periodically driven many-particle systems.

5.1.3 Deviations from instantaneous equilibrium

The exact differential equations in (5.5) and (5.8) form a closed system of first-order differential equations, and combining the equations with the particle-conserving mechanism outlined later in this chapter allows for the simulation of any system with Lindblad dynamics regardless of the driving rates. If, however, the driving is slow, we can simplify the mathematics considerably by assuming that $\partial_t R_t \simeq \hat{\mathsf{L}}_t R_t$ and by introducing the auxiliary variables

$$\delta \mathsf{N}_{\mathbf{mn}} \equiv \mathsf{N}_{\mathbf{mn}} - \bar{\mathsf{N}}_{\mathbf{mn}} = \mathrm{Tr}\{A^\dagger_{\mathbf{m},t} A_{\mathbf{n},t} (\varrho_t - R_t)\}, \tag{5.9}$$

which describe deviations from the instantaneous equilibrium populations, to approximate the dynamics with a closed system of first-order linear differential equations. Based on (5.5) and (5.8), the resulting mean-field equations of motion can then be written in matrix form as

$$|\delta\dot{\mathsf{N}}\rangle\!\rangle = \mathbb{W}_t|\delta\mathsf{N}\rangle\!\rangle. \tag{5.10}$$

Here, we have vectorized the deviations $|\delta\mathsf{N}\rangle\!\rangle \equiv \sum_{\mathbf{mn}} \delta\mathsf{N}_{\mathbf{mn}}|\mathbf{mn}\rangle\!\rangle$ and the corresponding occupations using an orthonormal column vector basis $\{|\mathbf{mn}\rangle\!\rangle\}$, which can be chosen arbitrarily. One option is to construct the basis vectors according to

$$|\mathbf{mn}\rangle\!\rangle \equiv \mathbf{e}_{m_x} \otimes \mathbf{e}_{m_y} \otimes \mathbf{e}_{n_x} \otimes \mathbf{e}_{n_y}, \tag{5.11}$$

where $\otimes$ denotes the Kronecker product [51] with the elements of the vectors $\mathbf{e}_k$ given by Kronecker deltas $[\mathbf{e}_k]_j = \delta_{jk}$. The notation $|\bullet\rangle\!\rangle$ is used to denote vectors expressed in this basis. We will also write $\langle\!\langle\bullet| \equiv |\bullet\rangle\!\rangle^\dagger$.

As the Hilbert space for the trapped gas is infinite-dimensional, the spectrum must be truncated in numerical implementations by including only the ℓ lowest modes in each spatial direction. Consequently, the basis vectors $|\mathbf{mn}\rangle\!\rangle$ span an ℓ^4-dimensional space. Written in terms of these vectors, the rate matrix $\mathbb{W}_t \equiv \mathbb{V}_t + \mathbb{X}_t$ can be split into diagonal

$$\mathbb{V}_t \equiv \sum_{\mathbf{mn}} -\left(\Gamma + \mathrm{i}\omega_t(m-n)\right)|\mathbf{mn}\rangle\!\rangle\langle\!\langle\mathbf{mn}|, \tag{5.12}$$

and off-diagonal contributions

$$\begin{aligned}\mathbb{X}_t \equiv \frac{\dot{\omega}_t}{4\omega_t}\sum_{\mathbf{kl}}|\mathbf{kl}\rangle\!\rangle \sum_{\nu=x,y}&\left(\sqrt{k_\nu(k_\nu-1)}\langle\!\langle\mathbf{k}_\nu^-\mathbf{l}| - \sqrt{(k_\nu+1)(k_\nu+2)}\langle\!\langle\mathbf{k}_\nu^+\mathbf{l}|\right)\\ &+\left(\sqrt{l_\nu(l_\nu-1)}\langle\!\langle\mathbf{k}\mathbf{l}_\nu^-| - \sqrt{(l_\nu+1)(l_\nu+2)}\langle\!\langle\mathbf{k}\mathbf{l}_\nu^+|\right).\end{aligned} \tag{5.13}$$

As the full rate matrices do not commute at different times, i.e., $\mathbb{W}_t\mathbb{W}_s \neq \mathbb{W}_s\mathbb{W}_t$ for $t \neq s$, the equations of motion (5.10) cannot simply be solved by exponentiating the integrated rate matrix. Instead, other methods are needed to solve the linear system with time-dependent coefficients. Here, we use time-ordering $\hat{\mathsf{T}}$ to formally solve the system and then use a first-order Dyson expansion for [39]

$$|\delta\mathsf{N}_{t+\Delta t}\rangle\!\rangle = \hat{\mathsf{T}}\exp\left[\int_t^{t+\Delta t}\mathrm{d}s\,\mathbb{W}_s\right]|\delta\mathsf{N}_t\rangle\!\rangle \simeq \left[\mathbb{1} + \int_t^{t+\Delta t}\mathrm{d}s\,\mathbb{W}_s\right]|\delta\mathsf{N}_t\rangle\!\rangle. \tag{5.14}$$

The series expansion is necessary to avoid evaluating the time-ordered exponential exactly, which is usually impossible. This expansion is also simple to implement and has a low computational cost, since there is no need to diagonalize the rate matrix for computing any exponentials.

It should be emphasized that under the approximation $\partial_t R_t \simeq \hat{\mathsf{L}}_t R_t$ the rate matrix $\mathbb{W}_t = \mathbb{W}_t[\omega_t]$ depends only on the mechanical driving ω_t and not on the temperature T_t or the chemical potential μ_t. Therefore, (5.14) can be used to find the limit cycle for the deviations from equilibrium. However, to calculate the thermodynamic power and efficiency, the occupations $\mathsf{N}_{\mathbf{mn}}$ need to be fully known along the entire limit cycle. As the equations of motion for the deviations $\delta\mathsf{N}_{\mathbf{mn}}$ are fully independent of the chemical potential, they can be solved before enforcing particle conservation so long as the initial values are chosen properly.

5.2 Effectively canonical systems

The mean-field equations of motion for the mean populations have been studied earlier within a canonical framework in [46], whose main results are recapped in Appendix C. Based on this prior work, it is possible to derive equations of motion using the canonical ensemble and have a particle-conserving master equation by using Lindblad operators of the form $\sum_{\mathbf{mn}} v_{\mathbf{mn},t} A^\dagger_{\mathbf{m},t} A_{\mathbf{n},t}$ with weights $v_{\mathbf{mn},t}$; the resulting non-linear equations of motion, however, rely heavily on approximations and do not form a closed set [46]. The grand-canonical approach used in this thesis, on the other hand, results in a closed system of linear differential equations, which can be written in matrix form as seen in Equation (5.10). The cost of this simplification is that the solution (5.14) to these linear equations does not identically conserve the mean total number of particles given by the diagonal sum $\sum_{\mathbf{n}} \mathsf{N}_{\mathbf{nn}} = \sum_{\mathbf{n}} \langle\!\langle \mathbf{nn}|\mathsf{N}\rangle\!\rangle$. The formal solution from Equation (5.14) cannot be used to solve the system over the entire cycle, because is it not known how the chemical potential, which appears explicitly in the instantaneous equilibrium occupations $\bar{\mathsf{N}}_{\mathbf{mn}} = \bar{\mathsf{N}}_{\mathbf{mn}}[\mu_t]$, should evolve in time for the particle number to remain constant. Therefore, to enforce the conservation law, the initial populations must be chosen to sum up to the fixed value $\mathcal{N}$ and the chemical potential to impede the net exchange of particles between the system and the reservoir.

To this end, let us assume that $\mathrm{Tr}\{N\varrho_t\} = \mathcal{N}$ is satisfied. As the total particle number operator is a constant of motion, the mean number of particles after a short time Δt later can be expanded using Taylor's theorem for

$$\mathrm{Tr}\{N\varrho_{t+\Delta t}\} = \mathrm{Tr}\{N\varrho_t\} + \mathrm{Tr}\{N\dot{\varrho}_t\}\Delta t + \mathcal{O}(\Delta t^2) = \mathcal{N} + J^\rho_t \Delta t + \mathcal{O}(\Delta t^2). \tag{5.15}$$

The second-order corrections can be ignored for sufficiently small Δt, implying that the total particle number is conserved between t and $t + \Delta t$ if the net particle current $J^\rho_t = \mathrm{Tr}\{(\hat{\mathsf{D}}^\dagger_t N)\varrho_t\}$ vanishes at all times. In terms of the mean-field variables, these conditions are met if

$$J^\rho_t = -\Gamma \sum_{\mathbf{n}} (\mathsf{N}_{\mathbf{nn},t} - \bar{\mathsf{N}}_{\mathbf{nn},t}) = 0 \Rightarrow \sum_{\mathbf{n}} \bar{\mathsf{N}}_{\mathbf{nn},t}[\mu_t] = \mathcal{N}. \tag{5.16}$$

As Equation (5.16) admits only one negative solution for the chemical potential, the particle number is conserved by the instantaneous equilibrium chemical potential.

Because the non-linear equation in (5.16) cannot be inverted analytically for μ_t, the time domain must be discretized into a large number of sub-intervals of length Δt. If $\Delta t/\mathcal{T}$ is sufficiently small, the driving protocols can be considered piecewise constant within these sub-intervals. It should also be noted that the initial values must be chosen in a consistent manner, meaning that the diagonals sum up to $\mathcal{N}$ and that the coherences satisfy $\mathsf{N}^*_{\mathbf{mn}} = \mathsf{N}_{\mathbf{nm}}$; the Hermiticity of the occupations is preserved at later points in time by the Lindblad dynamics [28].

5.3 Otto cycles

The outlined procedure for enforcing particle conservation is general and can be used to simulate the mean-field dynamics of any finite thermodynamic cycle. However, the matrix operations involving the ℓ^4-by-ℓ^4 matrix $\mathbb{W}_t$ as well as solving the non-linear algebraic equation (5.16) are computationally demanding. Due to the considerable computational resources needed for accurate results, we will now apply it to the quantum Otto cycle only to demonstrate that the mean particle number is conserved.

Throughout this thesis, we have emphasized the relative simplicity of the Otto cycle in comparison with other quantum thermodynamic cycles, and a major simplification can accordingly be made with the mean-field dynamics: the system can be considered unperturbed during the isochoric strokes, as the diagonal and off-diagonal elements are only coupled during the instantaneous expansion and compression strokes. This leaves the equations of motion analytically solvable with constant chemical potential values in the two isochores. Integrating over the instantaneous expansion and compression strokes at $t = 0$ and $t = \mathcal{T}/2$ modulo $\mathcal{T}$ yields the solution

$$\begin{aligned} |\mathsf{N}_{t^+}\rangle\!\rangle &\simeq |\bar{\mathsf{N}}_{t^+}\rangle\!\rangle + \left(\mathbb{1} + \int_{t^-}^{t^+} \mathrm{d}s\, \mathbb{W}_s\right) \left(|\mathsf{N}_{t^-}\rangle\!\rangle - |\bar{\mathsf{N}}_{t^-}\rangle\!\rangle\right) \\ &= |\bar{\mathsf{N}}_{t^+}\rangle\!\rangle + \left(\mathbb{1} \pm \log\left(1 + \frac{\Delta\omega}{\omega}\right)\mathbb{X}\right) \left(|\mathsf{N}_{t^-}\rangle\!\rangle - |\bar{\mathsf{N}}_{t^-}\rangle\!\rangle\right). \end{aligned} \tag{5.17}$$

Here, $+$ is for stroke 1 and $-$ for stroke 3 and the interval of integration is $[t-\varepsilon, t+\varepsilon]$ in the limit $\varepsilon \to 0^+$. We have also separated the off-diagonal part of the rate matrix $\mathbb{X}_t = (\dot{\omega}_t/\omega_t)\mathbb{X}$ into a product of time-dependent and time-independent parts.

The normalized populations of the ground state and the excited states are plotted in Figures 5.1 and 5.2 against time with the physical parameters chosen for demonstrative purposes to make the qualitative behavior of the mean occupations more pronounced. Figure 5.1 shows the qualitative behavior of the occupations under slow driving, and it can be observed that the populations of the included eigenstates are constantly relaxing towards their equilibrium values. As the system decoheres completely during the isochores, there are no jumps in the mean populations, which only couple with coherence elements during the adiabats. Notably, particle conservation is enforced by

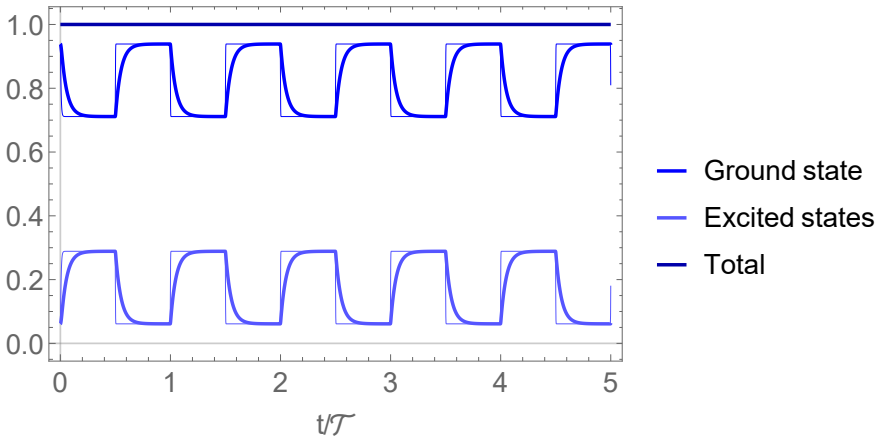

Figure 5.1: The time-evolution of the mean-field occupation fractions under slow driving. The mean occupations are constantly approaching their instantaneous equilibrium values exponentially, and there are no noticeable jumps as the system thermalizes during the isochores. The total particle number remains constant. Here, we have only included diagonals and coherences directly coupled with them whose eigenmode indices satisfy $\max\{m_x, m_y, n_x, n_y\} = 2$ as we have chosen $\ell = 3$. Note that the physical parameter values have been chosen for demonstrative purposes only and that the thin lines represent the equilibrium occupation fractions for the hot and cold strokes.

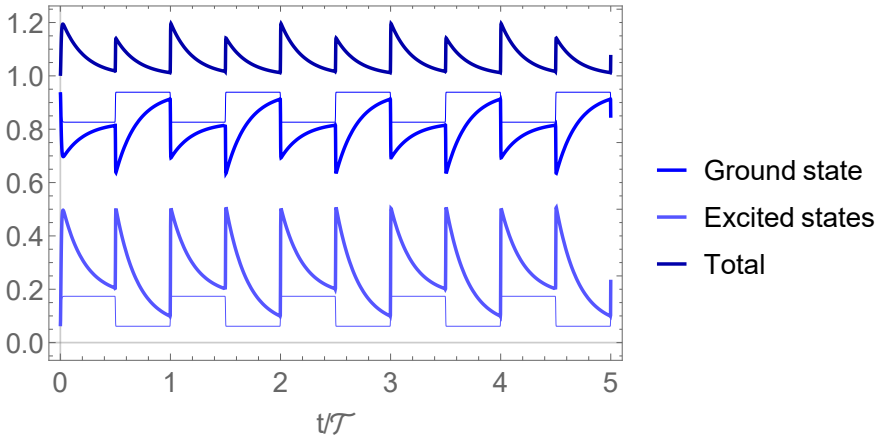

Figure 5.2: The time-evolution of the mean-field occupation fractions under fast driving. Now, the parameters are changed before the system equilibrates with the reservoirs, leading to coherence-induced jumps at the adiabats as well as the breakdown of the particle-conserving mechanism due to the truncation of the spectrum. Again, the parameter values have been chosen for demonstrative purposes only with $\ell = 3$.

the chemical potential protocol. Figure 5.2, on the other hand, shows the qualitative behavior of the mean populations in a fast driven system. Now, the instantaneous parameter switches happen before thermal equilibrium is reached, and the coupling between diagonal and off-diagonal elements leads to coherence-induced instantaneous changes in the eigenstate populations. However, now the total particle number is no longer conserved but experiences jumps during the adiabatic strokes, instead.

This failure is likely explained by the approximation we made in introducing the auxiliary variables $\delta\mathsf{N}_{\mathbf{mn}}$ to linearize the system: the instantaneous equilibrium distribution is not, in general, a solution to the Lindblad equation, and we have ignored first-order terms in the driving rates. In Otto cycles, this approximation is especially problematic as the driving protocols are step-like, leading to delta peaks in the driving rates at the jumps in the parameter values. These peaks would explain the sudden changes in the total particle number, depicted in Figure 5.2.

The observed deviations from expected behavior are also likely amplified by numerical effects: To simulate the dynamics efficiently, we have effectively reduced the system into a degenerate three-level system by considering only six eigenstates of the Hamiltonian as well as the elements describing coherence between these eigenstates; this is the smallest possible model for the two-dimensional trapped Bose gas where coherent effects can be observed. We have also ignored the off-diagonal elements that never couple with the diagonals. Truncating the spectrum involves dropping the terms proportional to $\mathsf{N}_{\mathbf{m}_\nu^+\mathbf{n}}$ and $\mathsf{N}_{\mathbf{mn}_\nu^+}$ in (5.8) from the equations of motion for the populations of highest excited states. With only a very limited amount of included energy levels, these coherence elements obtain non-negligible values from being directly coupled with low-energy eigenstates. These states are all macroscopically occupied, because the $\mathcal{N}$ particles are now distributed to only six levels instead of infinitely many. Ignoring the effects of coherence for the highest energy levels has non-negligible numerical consequences for the normalized excited-state population, which overcompensates for the sudden drops in the ground-state occupation. Together with the approximate linear equations of motion, this explains the violations of the particle conservation law as seen in Figure 5.2.

With only the bare minimum of $\ell = 3$ lowest eigenmodes needed for coherent effects to be observed included in the model, the truncation procedure also diminishes the values of thermodynamic quantities derived from changes in internal energy by increasing the contribution of the low-energy states to the population-weighted sum over the eigenenergies. As a result, the simulations used to generate the plots in 5.1 and 5.2 cannot be used to calculate the periodic power accurately due to the low-energy states with exaggerated populations dominating the average. Problems caused by the truncation can be mitigated by increasing the number of included energy levels, as the populations of high-energy states and their contributions to the thermodynamic quantities tend to be lower. Truncating the spectrum at an energy level with a negligible population would lead to smaller overshoots for the excited states during the adiabats.

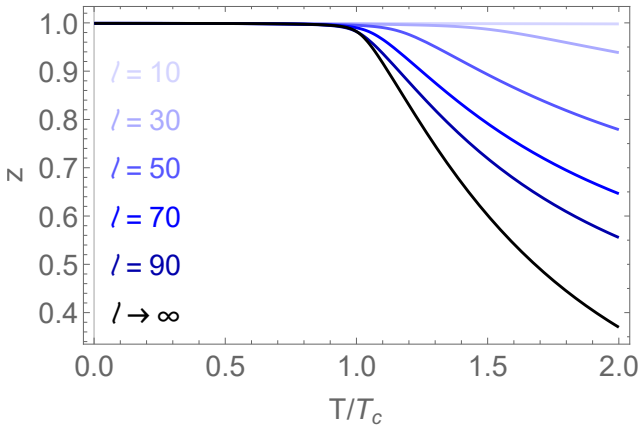

Figure 5.3: The pseudo-fugacity z for a truncated system against T/T_c for different truncation points ℓ with $\mathcal{N} = 1000$ fixed. The black line represents the real fugacity of the full system.

Increasing the number of included eigenmodes is, however, computationally demanding, and this number must be high before a truncated spectrum can be used to approximate the full spectrum. This is due to the critical role played by the pseudo-fugacity, which satisfies (5.16) for the truncated spectrum and which is plotted against temperature for various values of ℓ in Figure 5.3, in determining the equilibrium populations, which are numerically sensitive to changes in z especially near phase transitions. Hence, increased computational resources as well as more sophisticated hardware devoted to the problem are needed to calculate the periodic power reliably.

Furthermore, for a complete description of the dynamics, the full equations of motion must be solved while enforcing particle conservation. Working with the full dynamics, the utility of the auxiliary variables is somewhat lost as the equations of motion would inevitably involve derivatives of the chemical potential protocol, which is determined piecewise by extrapolation. Therefore, extending the basic methods outlined in this chapter for the inhomogeneous equations of motion

$$|\dot{\mathsf{N}}\rangle\rangle = \mathbb{W}_t|\mathsf{N}\rangle\rangle - \mathbb{V}_t|\bar{\mathsf{N}}\rangle\rangle, \tag{5.18}$$

would likely be a considerably simpler task on a technical level. This is left as a topic of future research.

Chapter 6

Concluding perspectives

In retrospect, the major physical result obtained in this thesis is the possibility of harnessing Bose-Einstein condensation to overcome quasi-classical bounds on performance even in non-interacting gases under equilibrium conditions. Ultimately, the observed quantum boost is the result of drastic changes in the ground-state occupation under small variations in temperature, induced by the condensation of particles, between the adiabatic strokes of the Otto cycle. This can be considered a reliable conclusion, as the results were derived using nothing but well-established thermostatistics. For a more complete understanding of the performance effects of Bose-Einstein condensation, the calculations could be repeated with interacting working fluids.

In the process of investigating the thermodynamic behavior of many-body Otto engines, we have also explored novel techniques for modelling the thermodynamics of many-body systems under periodic driving, and the condensation-induced performance enhancement was also detected using linear response. The many-body linear response theory outlined in this thesis is a significant extension of earlier results, because it allows for studying canonical many-particle systems within a grand-canonical framework. Since the Onsager coefficients cannot be determined exactly with particle-conserving Lindblad operators [46], the grand-canonical approach of this thesis is not only simpler on a technical level but also the only way to describe particle-conserving many-body Lindblad systems under periodic driving with the linear response theory of periodically driven open quantum systems.

Although linear response was able to not only reproduce the qualitative behavior of the exact work curves but also predict the performance boost in the condensate phase in comparison with the semiclassical limit, it was not able to fully describe the non-analytic behavior of power near the critical temperature. This failure is noteworthy, because linear response relies on the analytic behavior of equilibrium quantities under the variation of external parameters, thus making it possible that the effects of phase transitions during thermodynamic cycles might never be completely captured by lin-

ear response. To account for the non-analyticities more accurately, adiabatic response could be deployed. In adiabatic response, the state of system, now slowly driven, is expanded around the *instantaneous* equilibrium state, essentially assuming that the driving is slow enough for the system to be in constant equilibrium with the environment with only first-order corrections in the driving rates [52]. Potential difficulties with this approach include solving the self-consistency condition as required by the conservation of particles, because the adiabatic expansion would likely result in highly non-linear differential equations for the chemical potential.

Nevertheless, the behavior of the linear-response work is qualitatively consistent with results predicted by the equilibrium thermostatistics of trapped bosons, and even the transition from cubic to linear behavior near the condensation temperature is captured, which further demonstrates the utility of our effectively canonical linear response theory. The results from our linear-response calculations also show that the overall effect of coherence on performance is detrimental. These results, however, should not be considered indicative of the general performance effects of coherence, because coherence-induced power losses have been shown to be a universal feature of quantum heat engines in the linear-response regime. Combined with similar results recently derived for adiabatic response [16], this seems to indicate that coherence can only have conducive effects on the thermodynamic performance of quantum heat engines far from thermal equilibrium. Thus, while adiabatic response might capture the signatures of Bose-Einstein condensation more accurately than linear response, other methods are needed to investigate coherence comprehensively in many-body engines.

To this end, our mean-field approach could be implemented numerically on a much larger scale with sufficient computational resources devoted to the endeavor. Although the mean-field formalism was introduced to complement the linear response theory, no assumptions about the driving protocols were made in deriving the inhomogeneous equations of motion, and the behavior of quasi-classical and coherent contributions to the periodic power could be analyzed separately under arbitrary driving. In principle, this makes the equations valid for any driven-dissipative many-particle system with Lindblad dynamics. However, the number of included energy levels needed to describe the full system accurately might be too high for any practical implementations of the numerical procedure outlined in this thesis. In this case, the canonical approach introduced earlier in [46] could be improved using recent results [53]. The canonical equations of motion rely on Wick's theorem, which is only valid under equilibrium conditions in the grand-canonical ensemble [54]; in the canonical ensemble, Wick's theorem might be an accurate approximation for some parameter values but never exactly true, not even in equilibrium. Our equations could, however, be upgraded to account for thermal deviations from Wick's theorem in the canonical ensemble using recent results [53]. While these improvements would likely make it possible to apply linear or adiabatic response to canonical many-body systems, as these methods rely on equilibrium quantities, further research is needed to determine whether the effects of highly non-adiabatic driving can be accurately described even with these corrections.

Bibliography

[1] CLAYDEN J., GREEVES N. & WARREN S., *Organic Chemistry*, 2nd ed., Oxford University Press (2012).

[2] NELSON P., *Biological Physics*, 1st ed., W. H. Freeman Co. Ltd. (2007).

[3] PARRONDO J. M. R., HOROWITZ J. M. & SAGAWA T., Thermodynamics of information, *Nature Physics* **11**, 131-139 (2015).

[4] BLICKLE V. & BECHINGER C., Realization of a micrometer-sized stochastic heat engine, *Nature Physics* **8**, 143 (2011).

[5] MARTÍNEZ I. A., ROLDÁN É., DINIS L., PETROV D. & RICA R. A., Brownian Carnot engine, *Nature Physics* **12**, 67 (2015).

[6] KRISHNAMURTHY S., GHOSH S., CHATTERJI D., GANAPATHY R. & SOOD A. K., A micrometer-sized heat engine operating between bacterial reservoirs, *Nature Physics* **12**, 1134 (2016).

[7] ABAH O., ROSSNAGEL J., JACOB G., DEFFNER S., SCHMIDT-KALER F., SINGER K. & LUTZ E., Single-Ion Heat Engine at Maximum Power, *Physical Review Letters* **109**, 203006 (2012).

[8] ROSSNAGEL J., DAWKINS S. T., TOLAZZI K. N., ABAH O., LUTZ E., SCHMIDT-KALER F. & SINGER K., A single-atom heat engine, *Science* **352**, 325 (2017).

[9] SCOVIL H. E. D. & SCHULZ-DUBOIS E. O., Three-Level Masers as Heat Engines, *Physical Review Letters* **2**, 262 (1959).

[10] ALICKI R., The Quantum Open System as a Model of the Heat Engine, *Journal of Physics A: Mathematical and General* **12** (1979).

[11] ABE S. & OKUYAMA S., Role of the superposition principle for enhancing the efficiency of the quantum-mechanical Carnot engine, *Physical Review E* **85**, 011104 (2012).

[12] UZDIN R., LEVY A. & KOSLOFF R., Equivalence of Quantum Heat Machines, and Quantum-Thermodynamic Signatures, *Physical Review X* **5**, 03144 (2015).

[13] BRANDNER K., BAUER M., SCHMID M. T. & U. SEIFERT, Coherence-enhanced efficiency of feedback-driven quantum engines, *New Journal of Physics* **17**, 065006 (2015).

[14] KARIMI B. & PEKOLA J. P., Otto refrigerator based on a superconducting qubit - classical and quantum performance, *Physical Review B* **94**, 184503 (2016).

[15] BRANDNER K., BAUER M. & SEIFERT U., Universal Coherence-Induced Power Losses of Quantum Heat Engines in Linear Response, *Physical Review Letters* **119**, 170602 (2017).

[16] BRANDNER K. & SAITO K., Thermodynamic Geometry of Microscopic Heat Engines, arXiv:1907.06780 (2019).

[17] JARAMILLO J. BEAU M. & DEL CAMPO A., Quantum Supremacy of Many-Particle Thermal Machines, *New Journal of Physics* **18**, 075019 (2016).

[18] HALPERN N. Y., WHITE C. D., GOPALAKRISHNAN S. & REFAEL G., Quantum engine based on many-body localization, *Physical Review B* **99**, 024203 (2019).

[19] HARDAL A. U. C. & MÜSTECAPLIOĞLU Ö. E., Superradiant Quantum Heat Engine, *Scientific Reports* **5**, 12953 (2015).

[20] NIEDENZU W & KURIZKI G., Cooperative many-body enhancement of quantum thermal machine power, *New Journal of Physics* **20**, 113038 (2018).

[21] WANG J., HE J. & MA Y., Quantum heat engine based on trapped Bose gases: Its maximum efficiency can approach the Carnot value at finite power. Preprint, arXiv:1803.03734 (2018).

[22] EINSTEIN A., Quantentheorie des einatomigen idealen Gases, *Sitzungsberichte der Preussischen Akademie der Wissenschaften* **1**, 3 (1925).

[23] ANDERSON M. H., ENSHER J. R., MATTHEWS M. R., WIEMAN C. E. & CORNELL E. A., Observation of Bose–Einstein Condensation in a Dilute Atomic Vapor, *Science* **269**, 5221 (1995).

[24] DAVIS K. B., MEWES M. O., ANDREWS M. R., VAN DRUTEN N. J., DURFEE D. S., KURN D. M. & KETTERLE W., Bose-Einstein Condensation in a Gas of Sodium Atoms, *Physical Review Letters 75*, 3969 (1995).

[25] BLUNDELL S. J. & BLUNDELL K. M., *Concepts in Thermal Physics*, 2nd ed., Oxford University Press (2010).

[26] REHR J. J. & MERMIN N. D., Condensation of the Rotating Two-Dimensional Ideal Bose Gas, *Physical Review B* **1**, 3160 (1970).

[27] KOSLOFF R. & REZEK Y., The quantum harmonic Otto cycle, *Entropy* **19**, 136 (2017).

[28] BREUER H.-P. & PETRUCCIONE F., *The Theory of Open Quantum Systems*, Oxford University Press (2002).

[29] VORBERG D., WUSTMANN W., KETZMERICK R. & ECKARDT A., Generalized Bose-Einstein condensation into multiple states in driven-dissipative systems, *Physical Review Letters* **111** (2013).

[30] VORBERG D., WUSTMANN W., SCHOMERUS H., KETZMERICK R. & ECKARDT A., Non-equilibrium steady states of ideal bosonic and fermionic quantum gases, *Physical Review E* **92** (2015).

[31] LEYMANN H. A. M., VORBERG D., LETTAU T., HOPFMANN C., SCHNEIDER C., KAMP M., HÖFLING S., KETZMERICK R., WIERSIG J., REITZENSTAIN S. & ECKARDT A., Pump-power-driven mode switching in a microcavity device and its relation to Bose-Einstein condensation, *Physical Review X* **7** (2017).

[32] SCHNELL A., VORBERG D., KETZMERICK R. & ECKARDT A., High-temperature nonequilibrium Bose condensation induced by a hot needle, *Physical Review Letters* **119** (2017).

[33] SCHNELL A., KETZMERICK R. & ECKARDT A., On the number of Bose-selected modes in driven-dissipative ideal Bose gases, *Physical Review E* **97** (2018).

[34] VORBERG D., KETZMERICK R. & ECKARDT A., A unified theory for excited-state, fragmented, and equilibrium-like Bose condensation in pumped photonic many-body systems, *Physical Review A* **97** (2018).

[35] JASCHKE D., MONTANGERO S. & CARR L. D., One-dimensional many-body entangled open quantum systems with tensor network methods, *Quantum Science and Technology* **4**, 013001 (2018).

[36] BRANDNER K. & SEIFERT U., Periodic Thermodynamics of Open Quantum Systems, *Physical Review E* **93**, 062134 (2016).

[37] GIBBS J. W., *Elementary Principles of Statistical Mechanics*, Yale University Press (1902).

[38] LANDSBERG P. T., *Thermodynamics*, Interscience (1961).

[39] SAKURAI J.J., *Modern Quantum Mechanics*, Rev. ed., Addison-Wesley (1994).

[40] SCHWABL F., *Advanced Quantum Mechanics*, 3rd ed., Springer (2000).

[41] DULOCK V. A. & McINTOSH H. V., On the Degeneracy of the Two-Dimensional Harmonic Oscillator, *American Journal of Physics 33*, 109 (1965).

[42] ARFKEN G., WEBER H. J. & HARRIS F. E., *Mathematical Methods for Physicists*, 7th ed., Academic Press (2012).

[43] GORINI V., KOSSAKOWSKI A. & SUDARSHAN E. C. G., Completely positive dynamical semigroups of N-level systems, *Journal of Mathematical Physics* **17**, 821 (1976).

[44] LINDBLAD G., On the generators of quantum dynamical semigroups, *Communications in Mathematical Physics* **48**, 119 (1976).

[45] CALLEN H.B., *Thermodynamics and an Introduction to Thermostatistics*, 2nd ed., John Wiley & Sons (1985).

[46] PYHÄRANTA T., *Thermodynamics of non-equilibrium Bose-Einstein condensation in periodically driven systems* (special assignment at Aalto University).

[47] SPOHN H., Entropy Production for Quantum Dynamical Semigroups, *Journal of Mathematical Physics* **19**, 1227 (1978).

[48] WILCOX R. M., Exponential Operators and Parameter Differentiation in Quantum Physics, *Journal of Mathematical Physics* **8**, 962 (1967).

[49] KUBO R., TODA M. & HASHITSUME N., *Statistical Physics II - Nonequilibrium Statistical Mechanics*, Springer (1985).

[50] KAC V. & CHEUNG P., *Quantum Calculus*, Springer (2002).

[51] BYRON F. W. & Fuller R. W., *Mathematics of Classical and Quantum Physics*, Rev. ed., Dover Publications (2012).

[52] CAVINA V., MARI A. & GIOVANETTI V., Slow dynamics and thermodynamics of open quantum systems, *Physical Review Letters* **119**, 050601 (2017).

[53] SCHÖNHAMMER K., Deviations from Wick's theorem in the canonical ensemble, *Physical Review A* **96**, 012102 (2017).

[54] GIULIANI G. F. & VIGNALE G., *Quantum Theory of the Electron Liquid*, Cambridge University Press (2005).

Appendix A

Limit behavior of ideal engines

In this appendix, we derive expressions for bosonic thermostatistics at high and low temperatures. These results are depicted in the figures of Chapter 2.

A.1 High-temperature limit

The semiclassical behavior of bosonic fluids is recovered by replacing the Bose-Einstein distribution with the semiclassical Maxwell-Boltzmann statistics $\mathfrak{m}_n \equiv ze^{-\hbar\omega n/T}$ [25]. The chemical potential can then be solved from

$$\mathcal{N} \simeq \mathfrak{m}_0 + \int_0^\infty \mathrm{d}n\, g_n \mathfrak{m}_n = z\left[1 + \left(\frac{T}{\hbar\omega}\right) + \left(\frac{T}{\hbar\omega}\right)^2\right]. \tag{A.1}$$

As we assume that the energy levels form a quasi-continuum, $T \gg \hbar\omega$ and (A.1) can be solved approximately in the high-temperature limit for $z \simeq \mathcal{N}(\hbar\omega/T)^2$.

The internal energy similarly assumes the form

$$E/\hbar\omega \simeq z\left[1 + \left(\frac{T}{\hbar\omega}\right) + 2\left(\frac{T}{\hbar\omega}\right)^2 + 2\left(\frac{T}{\hbar\omega}\right)^3\right], \tag{A.2}$$

which can be approximated by neglecting the lower powers of temperature and plugging in the high-temperature fugacity for

$$E/\hbar\omega \simeq 2\mathcal{N}T. \tag{A.3}$$

This linear behavior in temperature is in perfect agreement with the classical equipartition theorem [25].

A.2 Low-temperature limit

In the thermodynamic limit, the chemical potential collapses to the ground-state energy at the critical temperature, below which the fugacity is $z \simeq 1$. Using the polylogarithm identity $\mathrm{Li}_s(1) = \zeta(s)$ [42], we can derive low-temperature expressions for the internal energy. Against T/T_c, the lower powers of $T/\hbar\omega$ can still be neglected in the thermodynamic limit as $T_\mathrm{c} \propto \sqrt{\mathcal{N}}$. Hence, the internal energy assumes the simplified low-temperature expression

$$E/\hbar\omega \simeq 2\left(\frac{T}{\hbar\omega}\right)^3 \zeta(3) = 2\left(\frac{T}{T_\mathrm{c}}\right)^3 \left(\frac{\mathcal{N}}{\zeta(2)}\right)^{3/2} \zeta(3). \tag{A.4}$$

This expression explains the cubic growth in temperature of both energy and work below the critical value.

Appendix B

Response coefficients

The integrated response coefficients from Equation (4.39) can be written as

$$\begin{aligned} \mathcal{D}^{\alpha\beta} &\equiv \sum_{s=-1}^{3} \mathscr{D}_s^{\alpha\beta} |s|! \left(\frac{T}{\hbar\omega}\right)^{s+1} \mathrm{Li}_s(z) \qquad \text{and} \\ \mathcal{C}^{ww} &\equiv \sum_{s=-1}^{3} \mathscr{C}_s^{ww} |s|! \left(\frac{T}{\hbar\omega}\right)^{s+1} \frac{\mathrm{Li}_{s+1}(z) - \mathrm{Li}_{s+1}(ze^{-2\hbar\omega/T})}{2\hbar\omega/T}, \end{aligned} \tag{B.1}$$

where the prefactors $\mathscr{D}_s^{\alpha\beta}$ and $\mathscr{C}_s^{\alpha\beta}$ can be read from Table B.1.

Table B.1: Prefactors for the coefficients in (B.1).

α	β	$\mathscr{D}_{-1}^{\alpha\beta}$	$\mathscr{D}_0^{\alpha\beta}$	$\mathscr{D}_1^{\alpha\beta}$	$\mathscr{D}_2^{\alpha\beta}$	$\mathscr{D}_3^{\alpha\beta}$
ρ	ρ	1	1	1	0	0
ρ	q	$-\mu$	$-\mu$	$\hbar\omega - \mu$	$\hbar\omega$	0
ρ	w	-1	-1	-2	-1	0
q	ρ	$-\mu$	$-\mu$	$\hbar\omega - \mu$	$\hbar\omega$	0
q	q	μ^2	μ^2	$\mu^2 - 2\hbar\omega\mu$	$(\hbar\omega)^2 - 2\hbar\omega\mu$	$(\hbar\omega)^2$
q	w	μ	μ	$2\mu - \hbar\omega$	$\mu - 2\hbar\omega$	$-\hbar\omega$
w	ρ	-1	-1	-2	-1	0
w	q	μ	μ	$2\mu - \hbar\omega$	$\mu - 2\hbar\omega$	$-\hbar\omega$
w	w	1	1	3	3	1
α	β	$\mathscr{C}_{-1}^{\alpha\beta}$	$\mathscr{C}_0^{\alpha\beta}$	$\mathscr{C}_1^{\alpha\beta}$	$\mathscr{C}_2^{\alpha\beta}$	$\mathscr{C}_3^{\alpha\beta}$
$\alpha \neq w$	$\beta \neq w$	0	0	0	0	0
w	w	6	6	14	9	1

Appendix C

Canonical mean-field dynamics

In this appendix, we briefly present the main results of [46], in which mean-field dynamics were studied within a canonical framework.

C.1 Canonical Lindblad equation

Within the canonical formalism, the Lindblad operators must be chosen such that the total particle number remains unchanged, e.g., by second-quantizing the ladder operators of the two-dimensional harmonic oscillator:

$$V_\nu \equiv \sum_{\mathbf{mn}} \langle \mathbf{m}|a_\nu|\mathbf{n}\rangle A^\dagger_{\mathbf{m}} A_{\mathbf{n}} = \sum_{\mathbf{n}} \sqrt{n_\nu + 1} A^\dagger_{(n_\nu, n_{\neq\nu})} A_{(n_\nu+1, n_{\neq\nu})}, \tag{C.1}$$

which satisfy the commutation identities

$$V_\nu R = R V_\nu e^{-\hbar\omega/T} \tag{C.2}$$

with the canonical equilibrium state $R \equiv e^{-H/T}/\mathrm{Tr}\{e^{-H/T}\}$. This follows from the transition rates satisfying the detailed-balance condition $\gamma^\dagger = \gamma e^{-\hbar\omega/T}$. As a result of the commutation identity and the detailed-balance condition, the canonical state R can be shown to be a stationary solution of the master equation.

C.2 Mean-field equations of motion

As with the grand-canonical ensemble, the equations of motion for the canonical mean occupations $\mathsf{n}^{\mathsf{l}}_{\mathbf{k}} \equiv \mathrm{Tr}\{A^\dagger_{\mathbf{k}} A_{\mathbf{l}} \varrho\}$ are derived using the Lindblad equation, leading to $\dot{\mathsf{n}}^{\mathsf{l}}_{\mathbf{k}} = -\langle \hat{\mathsf{H}} A^\dagger_{\mathbf{k}} A_{\mathbf{l}}\rangle + \langle \hat{\mathsf{D}}^\dagger A^\dagger_{\mathbf{k}} A_{\mathbf{l}}\rangle + \langle \partial_t (A^\dagger_{\mathbf{k}} A_{\mathbf{l}})\rangle$, where the adjoint dissipator is formed using the Lindblad operators V and $V^\dagger$. To break down the ensemble averages of the operator strings, we use Wick's theorem [54] to make the approximation

$$\langle A^\dagger_{\mathbf{k}} A_{\mathbf{l}} A^\dagger_{\mathbf{m}} A_{\mathbf{n}}\rangle \simeq \langle A^\dagger_{\mathbf{k}} A_{\mathbf{l}}\rangle \langle A^\dagger_{\mathbf{m}} A_{\mathbf{n}}\rangle + \langle A^\dagger_{\mathbf{k}} A_{\mathbf{n}}\rangle \langle A^\dagger_{\mathbf{m}} A_{\mathbf{l}} + \delta_{\mathbf{ml}}\rangle, \tag{C.3}$$

where we have only included particle-conserving terms. As we work with the canonical ensemble, the approximation in (C.3) is not exact even in equilibrium. The full equations of motion assume the mean-field form

$$\begin{aligned}
\dot{\mathsf{n}}_{\mathbf{i}}^{\mathbf{j}} \simeq \sum_{\mathbf{l};\nu}^{\infty} \sqrt{l_\nu^+} \Bigg[& \frac{\gamma^\dagger}{2} \Big(\sqrt{i_\nu^-} (\mathsf{n}_{\mathbf{i}_\nu^-}^{\mathbf{j}} \mathsf{n}_{\mathbf{l}_\nu^+}^{\mathbf{l}} + \mathsf{n}_{\mathbf{i}_\nu^-}^{\mathbf{l}} \mathsf{n}_{\mathbf{l}_\nu^+}^{\mathbf{j}}) - \sqrt{j_\nu^+} (\mathsf{n}_{\mathbf{i}}^{\mathbf{j}_\nu^+} \mathsf{n}_{\mathbf{l}_\nu^+}^{\mathbf{l}} + \mathsf{n}_{\mathbf{i}}^{\mathbf{l}} \mathsf{n}_{\mathbf{l}_\nu^+}^{\mathbf{j}_\nu^+}) \\
& + \sqrt{j_\nu} (\mathsf{n}_{\mathbf{l}}^{\mathbf{l}_\nu^+} \mathsf{n}_{\mathbf{i}}^{\mathbf{j}_\nu^-} + \mathsf{n}_{\mathbf{l}}^{\mathbf{j}_\nu^-} \mathsf{n}_{\mathbf{i}}^{\mathbf{l}_\nu^+}) - \sqrt{i_\nu^+} (\mathsf{n}_{\mathbf{l}}^{\mathbf{l}_\nu^+} \mathsf{n}_{\mathbf{m}_\nu^+}^{\mathbf{j}} + \mathsf{n}_{\mathbf{l}}^{\mathbf{j}} \mathsf{n}_{\mathbf{m}_\nu^+}^{\mathbf{l}_\nu^+}) \Big) \\
& + \frac{\gamma}{2} \Big(\sqrt{i_\nu^+} (\mathsf{n}_{\mathbf{i}_\nu^+}^{\mathbf{j}} \mathsf{n}_{\mathbf{l}}^{\mathbf{l}_\nu^+} + \mathsf{n}_{\mathbf{i}_\nu^+}^{\mathbf{l}_\nu^+} \mathsf{n}_{\mathbf{l}}^{\mathbf{j}}) - \sqrt{j_\nu} (\mathsf{n}_{\mathbf{i}}^{\mathbf{j}_\nu^-} \mathsf{n}_{\mathbf{l}}^{\mathbf{l}_\nu^+} + \mathsf{n}_{\mathbf{i}}^{\mathbf{l}_\nu^+} \mathsf{n}_{\mathbf{l}}^{\mathbf{j}_\nu^-}) \\
& + \sqrt{j_\nu^+} (\mathsf{n}_{\mathbf{l}_\nu^+}^{\mathbf{l}} \mathsf{n}_{\mathbf{i}}^{\mathbf{j}_\nu^+} + \mathsf{n}_{\mathbf{l}_\nu^+}^{\mathbf{j}_\nu^+} \mathsf{n}_{\mathbf{i}}^{\mathbf{l}}) - \sqrt{i_\nu} (\mathsf{n}_{\mathbf{l}_\nu^+}^{\mathbf{l}} \mathsf{n}_{\mathbf{i}_\nu^-}^{\mathbf{j}} + \mathsf{n}_{\mathbf{l}_\nu^+}^{\mathbf{j}} \mathsf{n}_{\mathbf{i}_\nu^-}^{\mathbf{l}}) \Big) \Bigg] \\
& + \gamma^\dagger \Big(\sqrt{i_\nu j_\nu} \mathsf{n}_{\mathbf{i}_\nu^-}^{\mathbf{j}_\nu^-} - \frac{i_\nu^+ + j_\nu^+}{2} \mathsf{n}_{\mathbf{m}}^{\mathbf{n}} \Big) + \gamma \Big(\sqrt{i_\nu^+ j_\nu^+} \mathsf{n}_{\mathbf{m}_\nu^+}^{\mathbf{j}_\nu^+} - \frac{i_\nu + j_\nu}{2} \mathsf{n}_{\mathbf{i}}^{\mathbf{j}} \Big) \\
& + \frac{\dot{\omega}_t}{4\omega_t} \Big(\sqrt{i_\nu i_\nu^-} \mathsf{n}_{\mathbf{i}_\nu^{--}}^{\mathbf{j}} - \sqrt{i_\nu^+ i_\nu^{++}} \mathsf{n}_{\mathbf{i}_\nu^{++}}^{\mathbf{j}} + \sqrt{j_\nu j_\nu^-} \mathsf{n}_{\mathbf{i}}^{\mathbf{j}_\nu^{--}} - \sqrt{j_\nu^+ j_\nu^{++}} \mathsf{n}_{\mathbf{j}}^{\mathbf{j}_\nu^{++}} \Big) \\
& + \mathrm{i}\omega(i - j) \mathsf{n}_{\mathbf{i}}^{\mathbf{j}},
\end{aligned} \tag{C.4}$$

where $\mathbf{n}_\nu^+ \equiv (n_\nu + 1, n_{\neq\nu})$, $\mathbf{n}_\nu^{++} \equiv (n_\nu + 2, n_{\neq\nu})$ with n, n_ν^+, n_ν^{++} denoting the component sums. With these equations, it becomes possible to show that the mean-field approximation preserves the conservation of the total particle number by substituting $\mathbf{i} = \mathbf{j}$ and performing a change of indices in the positive terms of the infinite sums. However, with constant driving protocols, the stationary solutions of (C.4) are not stationary solutions of the exact equations of motion, which are given by canonical equilibrium statistics, due to the mean-field approximation in (C.3).

C.3 Linear response

Although the linear-response formalism from [36] can technically be applied to canonical many-body systems, it can be observed using bosonic commutation relations that the superoperator exponentials involving $\hat{\mathsf{L}}^\ddagger$ do not converge into simple expressions as they do in the grand-canonical framework. The calculations are simple but exceedingly long and cumbersome. Therefore, we will not write them out here. The basic idea is to consider terms with the prefactors γ or $\gamma^\dagger$ separately, as they cannot cancel each other out away from equilibrium, and apply the superoperator $\hat{\mathsf{L}}^\ddagger$ to operators of the form $\sum_{\mathbf{n}} \alpha_{\mathbf{n}} A_{\mathbf{n}}^\dagger A_{\mathbf{n}}$, which form the bulk of the perturbation operators. Each application of the superoperator increases the length of the string of Fock-space operators by two, thus leading to the expression exploding. Hence, the canonical linear-response formalism cannot be used to study such many-body systems as the ones considered in this thesis without introducing additional approximations.